Imbibition of a liquid droplet on a deformable porous substrate

Daniel M. Anderson[a)]
Department of Mathematical Sciences, George Mason University, Fairfax, Virginia 22030

(Received 20 December 2004; accepted 14 June 2005; published online 2 August 2005)

We consider the imbibition of a liquid droplet into a deformable porous substrate. The liquid in the droplet is imbibed due to capillary suction in an initially dry and undeformed substrate. Deformation of the substrate occurs as the liquid fills the pore space. In our model, a pressure gradient in the liquid across the developing wet substrate region induces a stress gradient in the solid matrix which in turn leads to an evolving solid fraction and hence deformation. For axisymmetric droplets, we assume that the imbibition and substrate deformation at a given radial position are one-dimensional (in the vertical direction). The coupling to the droplet geometry leads to axisymmetric configurations for the deformed wet substrate. We show that the model chosen to describe the dynamics of the liquid droplet, based in this case on existing models developed for droplet spreading on rigid porous substrates, has little influence on the resultant swelling or shrinking of the substrate—these general trends can be effectively predicted by a one-dimensional imbibition and deformation model—but does strongly influence the details of the wet substrate shape. We characterize these predictions and in some cases can obtain analytical solutions for the evolution.
 [DOI: 10.1063/1.2000247]

I. INTRODUCTION

In this paper we develop a model for the imbibition of a liquid droplet into a deformable porous substrate. The motivation behind this work comes from the inkjet printing industry although the model we develop is general in nature and may be suitable for more simple systems such as a pure fluid penetrating into a dry sponge. Our interest here is the interaction between a fluid droplet and the receiving substrate (paper, film, etc.) from the point at which the droplet is in static contact with the substrate. The present study builds on existing models for imbibition of droplets into rigid substrates and models for one-dimensional deformation.

Imbibition of fluid into a rigid porous substrate is both a classical problem and a problem of current technological interest. The widely used Lucas–Washburn model[1] for liquid imbibition into a porous material is based on the assumption that the porous material can be modeled as a collection of vertically arranged cylindrical capillary tubes. The flow through each capillary tube is taken as Poiseuille flow subject to a pressure drop from one end of liquid column to the other. For liquid penetration due to capillary pressure in the tubes, a $t^{1/2}$ power law characterizes the depth of penetration into the porous material.

Recently, Clarke *et al.*[2] described droplet spreading and imbibition using experimental and analytical techniques. The experiments were conducted using a picoliter spreading and absorption instrument that produced droplets with an inkjet printer head. The liquid droplets under consideration included water and an aqueous solution of glycerol and hexelene glycol. The substrates were microporous filter membranes with mean pore diameters on the order of 0.1 μm. Spreading was modeled by an equation, previously applied to spreading on smooth impermeable substrates,[3] relating the speed of the contact line to the contact angle. The penetration was assumed to be of Lucas–Washburn-type, characterized by one-dimensional Darcy flow into a rigid substrate where the pressure gradient was given by the capillary pressure divided by the length of the filled pore space. Their observations included situations in which the droplet spreads initially before ultimately receding and being absorbed completely into the substrate. The rate of imbibition was strongly dependent on the wetting characteristics of the fluid and the substrate (e.g., the imbibition time for water was four orders of magnitude longer than the lower surface tension aqueous solution).

Holman *et al.*[4] examined the spreading and infiltration of inkjet-printed aqueous polymeric droplets (54- and 63-μm diameter) on a rigid porous ceramic surface (typical mean pore size of 0.1 μm). A spreading model with empirically determined parameters and a Washburn infiltration model were used to model the droplet dynamics. In this system the spreading and infiltration occur on the same time scale. The maximum extension of the droplet was found to depend on the characteristics of the substrate.

Davis and Hocking[6] examined a variety of different models for spreading and imbibition on porous membranes and substrates. These included cases of perfect and imperfect wetting on completely saturated substrates. The flow in the substrate was described by Darcy's law. They considered the partially saturated case in which the wetted portion of the substrate was assumed to extend to the bottom of the substrate (which was modeled as an impermeable boundary) and the boundary between saturated and unsaturated connected the top and bottom of the substrate. Davis and Hocking[7] adopt their previous results[6] to model the spreading above an initially dry porous substrate. As in the Lucas–Washburn description, the substrate was assumed to be made up of verti-

[a)]Electronic mail: danders1@gmu.edu

cally oriented capillaries, in which no "cross linking" of the capillaries in the substrate occurred. With this one-dimensional (1D) penetration model they calculated penetration shapes as a function of time. The contact-line speed of the droplet on the substrate surface was found to be nonmonotonic with respect to the contact angle; they concluded that no analogous "Tanner-law"-type result applies to spreading over dry permeable substrates. In contrast, Clarke *et al.*[2] have used such a condition and obtain agreement with their experiments. Consequently, as discussed below in more detail, we shall investigate the predictions of both the Davis and Hocking model as well as the Clarke *et al.* model in the context of a deformable substrate.

Starov *et al.*[8] investigated the spreading of liquid droplets over porous substrates saturated with the same liquid. They modeled the liquid in the porous substrate using Brinkman's equation. There was no net penetration of the liquid droplet since the substrate was saturated, however, liquid exchange between the droplet and porous substrate was reported to be important. Experiments were also undertaken using silicone oils on substrates of average pore size 0.25 μm and porosity of approximately 0.75. Both theory and experiment indicated that a power law governing the radial spreading applied to the droplet evolution.

Droplet spreading on rigid porous surfaces has also recently been examined by Seveno *et al.*,[9] who used molecular dynamics simulations to describe the dynamics of a droplet over a single capillary tube. Their numerical simulations for this problem provided a validation for a model based on Lucas–Washburn dynamics. Their generalization to multiple noninterconnecting pores characterized both the initial spreading and eventual receding/imbibition of the droplet.

An alternative to Darcy-type or Lucas–Washburn capillary flow models for porous substrates is a diffusion-type model appropriate for polymer matrix substrates. For example, Oliver, Agbezuge, and Woodcock[10] described a model for drying inkjet drops based on Fickian diffusion for the ink absorption into the paper. They included simple models for evaporation from the liquid droplet and evaporation after complete penetration occurred. Swelling of the paper was not directly considered, however, such effects were partially accounted for through the use of experimentally determined diffusion coefficients. They also conducted experiments using a water-based ink on substrates including three different office bond papers, and coated and uncoated Mylar (Xerox) transparency films. Measurements were made of volume, contact angle, contact line circularity, and contact area as a function of time. They suggested that local capillary wicking as well as fiber swelling may play important roles for the ink drops on the paper substrates considered. The problem of liquid imbibition into paper during coating has also been examined through the use of pore network models.[11]

Selim *et al.*[5] examined drying of water-based inks on plain paper and developed a diffusion-based model for evaporation of the liquid and used a Lucas–Washburn model for the penetration into the paper. Using their model and experimental evidence for two different paper types ("acid-made rosin-sized paper" and "alkaline-made synthetic-sized paper") they found generally that the time scale for penetration is much smaller than that for evaporation. Specifically, they reported that for the "rosin-sized paper (the least penetrating paper)" the mass loss in a liquid film due to penetration into the porous substrate was about 100 times greater than the mass loss into the vapor phase due to evaporation. They comment that the role of evaporation can be increased for nonwater-based inks.

The deformation of a porous material has also been a long-studied problem that has attracted the attention of researchers in fields ranging from geophysics,[12] soil science,[13–20] infiltration processes,[21–25] paper and printing industries[26,27] and medical science.[28–37] These include situations in which imbibition occurs and also situations of fully saturated media in which capillarity is of secondary or no importance. Deformation in systems such as glassy polymers, which we do not consider here, can be described by Case II diffusion[38] wherein the penetration of organic material into a polymer matrix, at a sharply defined diffusion front, swells the polymer.

Early descriptions of deformable porous media include the work of Biot[39] on soil settlement, in which fluid flow based on Darcy's law is coupled to a linear elasticity model for the solid deformation. Solutions for soil consolidation in one dimension as well as two dimensions under permeable[40] and impermeable[41] rectangular loads were obtained.

Chen and Scriven[26] modeled a roll applicator process appropriate for coating flows in the paper and printing industry. Their model treated the flow in the deformable receiving porous region, the flow external to the porous region, and additionally addresses the effects of air compression and trapped air in the substrate. Flow was driven both by capillary and external pressures. Substrate deformation was modeled by assuming that the liquid pressure in the pore space and the thickness of the compressed substrate were linearly related. Geometrical considerations then related the substrate thickness to the local solid fraction.

In the model we develop here for the droplet geometry, we adopt the formulation for liquid penetration and substrate deformation of Preziosi *et al.*,[22] who studied the infiltration of a liquid into porous preforms in the industrial process of injection molding. We describe our adaption of their model in more detail below.

The inkjet printing problem involves a number of fluid dynamic effects, most of which we do not address here. We shall neglect the effects of evaporation of the fluid. We consider only a mechanical interaction between the fluid and the substrate and neglect chemical properties of either the fluid or substrate. Additionally, we shall assume that the liquid droplet is initially at rest so that the dynamics of droplet formation, impact and possible merging of droplets can be neglected. Other issues of importance in the inkjet printing problem include radial capillary penetration[42,43] and configurations with a relatively thin substrate[6,44] in which the penetrating liquid reaches the bottom of the substrate. The focus of the present work will be on a configuration in which penetration occurs only in the vertical direction in a substrate whose thickness is much greater than the maximum penetration depth of the fluid. We further assume that the fluid pen-

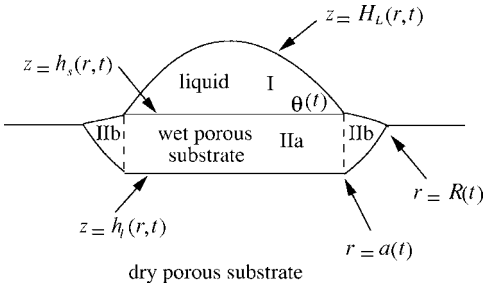

FIG. 1. The basic droplet/substrate geometry.

etrates along a well-defined front and completely displaces the existing air in the pore space, so that the effects of partial saturation on the permeability of the media are neglected.

With the complex physical processes of inkjet printing technology in mind, we shall direct our attention to the rather modest goal of developing a model for the imbibition of a pure liquid droplet into a deformable porous substrate. As we shall see, despite the long list of simplifications given above, there is still a significant level of complexity in this problem.

In Sec. II we describe the basic model geometry and outline the governing equations applied in the deformable wet substrate. In Sec. III we describe a reduced set of governing equations for one-dimensional imbibition and deformation including boundary conditions appropriate for finite liquid volumes characteristic of the droplet geometry. Here we also describe similarity solutions and numerical solutions for the wet substrate region. In Sec. IV we describe how the liquid droplet evolution couples to the dynamics of the wet substrate region. Here we give results for three different liquid droplet evolution models coupled to two different model boundary conditions for a total of six different characterizations of the droplet substrate interaction problem. We identify the key parameters in the imbibition and deformation process. In Sec. V we summarize the results and give concluding remarks.

II. MODEL DESCRIPTION

We consider an axisymmetric liquid droplet initially at rest on a dry porous substrate. The fluid in the droplet is imbibed by the substrate due to capillary suction in the pore space of the substrate. We consider also only sufficiently small droplets so that the effects of gravity can be neglected. There is an additional overpressure in the liquid droplet due to curvature of the liquid–vapor interface whose contribution to the overall penetration problem is neglected. This assumption is valid when the typical pore size in the substrate is much smaller than the droplet diameter. Deformation of the substrate occurs as a consequence of the fluid penetration. Specifically, deformation of the substrate is assumed to occur as an isotropic elastic response to the pressure exerted on the solid matrix by the fluid occupying the pore space. Imbibition continues until the liquid droplet volume is depleted. Simultaneous substrate deformation occurs during the imbibition process and further deformation may occur after the liquid is completely imbibed.

The geometry of the system is shown in Fig. 1. The fluid droplet occupies a region we denote by Region I. The position of the liquid–vapor interface is given by $z=H_L(r,t)$, the contact line position by $a(t)$, the contact angle (with respect to the tangent to the substrate beneath the fluid at the contact line) by $\theta(t)$ and the volume of fluid contained in the liquid droplet by $V_L(t)$. We assume that the substrate is infinitely deep and has initially a planar upper boundary at $z=0$. For $t>0$ the fluid in the droplet penetrates into the initially dry substrate. The region occupied by the wet porous substrate is defined above by $z=h_s(r,t)$ (the upper surface of the substrate) and below by the vertical penetration depth $z=h_l(r,t)$. This region is assumed to extend to a location $r=R(t)$ along the top of the substrate. We distinguish two regions within the wet porous substrate. Region IIa is the interior region directly underneath the liquid droplet $[0\leqslant r\leqslant a(t)]$ and Region IIb is the exterior region above which the overlying fluid has been completely imbibed $[a(t)\leqslant r\leqslant R(t)]$. In the one-dimensional characterization of the substrate deformation we develop below, these two regions are distinct from a modeling point of view in that they experience different boundary conditions at their upper surfaces. The whole configuration then is defined by a liquid region (the liquid droplet), a wet, deformable porous substrate and a dry, rigid porous substrate. Our aim is to develop a model for the evolution of the liquid droplet into the porous substrate and the subsequent deformation of the substrate.

The model for the liquid evolution above the porous substrate can be addressed by implementing any number of existing models for the spreading of liquid droplets on rigid porous substrates. Davis and Hocking,[6,7] for example, have derived an evolution equation in a lubrication limit and in addition to numerical solutions have identified simple quasi-steady solutions in which the droplet maintains a parabolic shape dominated by surface tension. In contrast to the case of liquid droplet spreading on an impermeable substrate, Davis and Hocking[7] concluded that there is no Tanner-type law relating the contact angle to the contact line speed for a droplet spreading on a porous substrate. In particular, they specifically identify that the apparent contact angle is not a single-valued function of the contact line speed. In contrast, Clarke *et al.*[2] have implemented a model for droplet spreading on a porous substrate which *does* employ a prescribed monotonic relationship between the contact line speed along the porous substrate and the contact angle. This dynamic model for the contact line was coupled to a spherical cap approximation for the liquid–vapor interface shape and a Lucas–Washburn penetration law. The results of this model were compared favorably with experimental measurements. Another approach by Denesuk *et al.*[45,46] has been to examine the two limiting cases of a fixed contact angle ("decreased drawing area") and a fixed contact line ("constant drawing area"). In the present work, we do not attempt to resolve these different views. Instead, we shall investigate a number of these liquid droplet models with the objective of keeping the description of the liquid droplet relatively simple so that our focus can be directed on the deformation of the porous substrate. For this reason, we consider only scenarios in which the footprint of the liquid droplet decreases monotonically in time [the one-dimensional imbibition model then

also implies that $R(t)=R_0$ for all time]. This excludes the scenario in which the liquid droplet spreads initially before receding. For droplets that recede monotonically in time, we shall find that the deformed substrate underneath the liquid droplet (i.e., in Region IIa) is always planar. Specific details on these models are given in Sec. IV.

We now turn our attention to the porous substrate. We shall assume that when the porous substrate is dry it is rigid and has a constant solid fraction ϕ_0. We further assume that the fluid penetrates along a well-defined front and completely displaces the existing air in the pore space, so that the effects of partial saturation on the permeability of the media can be neglected. We assume that the air moving through the dry porous substrate meets with no resistance and hence its effect on the motion of the liquid phase is negligible. Consequently, our primary objective will be to formulate governing equations that apply in the wet porous substrate and the associated interfacial conditions at the penetration front and at the deformed substrate surface. The model we adopt here follows closely existing substrate deformation models used by a number of authors,[12,21,33,47] which have been developed with a variety of applications in mind. The present description follows most closely the model of Preziosi, Joseph, and Beavers.[22] We describe our adaptation of this model to the present context below.

The variables of interest in the wet porous medium are the solid volume fraction ϕ, the velocity of the liquid phase $\vec{u}_l$, the velocity of the solid phase $\vec{u}_s$, the liquid pressure p and the stress in the solid $\boldsymbol{\sigma}$. Mass balance arguments applied to the solid and liquid phases under the assumption that the density of each phase is constant lead to the two continuity equations

$$\frac{\partial \phi}{\partial t} + \nabla \cdot (\phi \vec{u}_s) = 0, \tag{1}$$

$$\frac{\partial \phi}{\partial t} - \nabla \cdot [(1-\phi)\vec{u}_l] = 0. \tag{2}$$

The relative velocity $\vec{u}_l - \vec{u}_s$ is related to the liquid pressure gradient through Darcy's law given by

$$\vec{u}_l - \vec{u}_s = -\frac{K(\phi)}{(1-\phi)\mu} \nabla p, \tag{3}$$

where $K(\phi)$ is the permeability which is taken to be a function of the local solid volume fraction, μ is the dynamic viscosity of the fluid, and the factor $1-\phi$ (porosity) enters because Darcy's law applies to the volume flux. We specify the liquid and solid velocity vectors in terms of axisymmetric (r,z) components as $\vec{u}_l=(u_l,w_l)$ and $\vec{u}_s=(u_s,w_s)$. As described by Preziosi *et al.* these equations couple to momentum balances for the liquid and solid constituents. A reduced form of these combined momentum equations states that a stress equilibrium is maintained in the wet substrate. In particular, there is a balance of the stress in the solid with the pressure exerted by the surrounding liquid expressed by

$$0 = -\nabla p + \nabla \cdot \boldsymbol{\sigma}, \tag{4}$$

where $\boldsymbol{\sigma}$ is the excess stress tensor for the fluid–solid mixture and p is the pressure in the liquid phase. Even with this simplification, which, among other things neglects inertial effects, there is an important question of how one models the stress $\boldsymbol{\sigma}$. Preziosi *et al.* suggested a number of models for $\boldsymbol{\sigma}$ including modeling the solid as a Voight–Kelvin solid or as an anelastic material. We adopt the assumption that the solid can be treated as an isotropic elastic material where the stress tensor is taken to have the form

$$\boldsymbol{\sigma} = \sigma(\phi)\mathbf{I}, \tag{5}$$

where the σ is assumed to be a function of the solid volume fraction alone, $\sigma(\phi)$. Preziosi *et al.* have justified this for the one-dimensional case. We apply it here in higher dimensions, although in the simplification that follows below, our deformation model will be reduced to one-dimensional deformation. Barry and Aldis[33] employ an equivalent one-dimensional model for the stress. A similar approach was also adopted by Fitt *et al.*,[27] who took the substrate deformation to be one-dimensional and expressed the stress as a function of the solid fraction. Both Preziosi *et al.* and Sommer and Mortensen[21] make use of an empirically determined $\sigma(\phi)$ relation for their calculations. Spiegelman[12] adopts the same stress equilibrium, but assumes that the stress in the solid is that of a compressible, highly viscous fluid.

Boundary conditions at the liquid penetration front $z=h_l(r,t)$ include

$$\vec{u}_l \cdot \hat{n} = \frac{1}{\sqrt{1+(\partial h_l/\partial r)^2}} \frac{\partial h_l}{\partial t}, \tag{6}$$

$$p = p_A + p_c. \tag{7}$$

The first condition states that the geometric position of the penetration front moves with the normal fluid velocity there. The second is a condition on the fluid pressure involving the capillary pressure p_c and atmospheric pressure p_A. The capillary pressure p_c can be thought of as that used by Davis and Hocking[7] for one-dimensional capillaries $-\gamma \cos\theta/b$ (where γ is the surface tension, θ is the contact angle in the capillary and b is the capillary half-width), or more generally as $-S_f \gamma \cos\theta$ where S_f is the total surface area of solid–liquid interface per unit volume;[23] we treat p_c as a given constant in the present work.

The boundary conditions on the wet substrate–liquid interface $z=h_s(r,t)$ for $0 \leqslant r \leqslant a(t)$ are

$$\vec{u}_s \cdot \hat{n} = \frac{1}{\sqrt{1+(\partial h_s/\partial r)^2}} \frac{\partial h_s}{\partial t}, \tag{8}$$

$$p = p_A + p_L(t), \tag{9}$$

$$\sigma = 0, \tag{10}$$

where p_L is the pressure in the liquid droplet at the interface and is generally a function of time. The first condition states that the deformed boundary of the substrate moves with the normal solid velocity there. The second condition specifies

the pressure at the top of the wet substrate as that associated with the liquid droplet. Here this arises due to surface tension and the curvature of the liquid-vapor interface, but more generally involves effects due to gravity and/or an externally applied pressure. As mentioned earlier, we shall assume that the capillary pressure in the pore space is the dominant pressure (i.e., $|p_c| \gg |p_L|$). The third condition states that the interface between the wet substrate–liquid droplet is stress free.

In the present investigation we examine two possible models for the evolution of the wet substrate–vapor interface $z=h_s(r,t)$ for $a(t) \leqslant r \leqslant R(t)$. In the first case (Case A), we assume that the state of the substrate is "frozen" in place at a given radial position once the liquid droplet recedes past that position. In the second case (Case B), we assume that the wet substrate–vapor interface continues to evolve in such a way that the solid moves with the fluid there to maintain a wet substrate–vapor interface; no "puddles" form at the top of the substrate nor does the substrate dry out. This translates to the boundary condition $\vec{u}_l = \vec{u}_s$. The interface position $h_s(r,t)$ continues to evolve according to Eq. (8).

In addition to the above equations and boundary conditions for the wet substrate region, there is a global mass balance equation for the liquid in the droplet region and in the wet substrate region. We denote by $V_S(t)$ the geometric volume occupied by the fluid which has penetrated the solid, defined as

$$V_S(t) = 2\pi \int_0^{R(t)} r[h_s(r,t) - h_l(r,t)]dr. \tag{11}$$

The actual volume of fluid $V^*(t)$ occupying the pore space must be adjusted by accounting for the total amount of solid occupying the same volume. That is,

$$V^*(t) = 2\pi \int_0^{R(t)} \int_{h_l}^{h_s} [1 - \phi(r,z,t)] r \, dz \, dr. \tag{12}$$

In terms of this, we have a global conservation equation $V_0 = V_L(t) + V^*(t)$, where V_0 represents the initial volume of fluid which is constant in time (e.g., we do not consider the effects of mass loss due to evaporation).

III. ONE-DIMENSIONAL SUBSTRATE DEFORMATION SOLUTIONS

We focus on a droplet/substrate geometry in which the horizontal length scale R_0 associated with the wet substrate is much larger than the vertical length scale H_0 in the wet substrate. Additionally, we note that the pressure scale in the wet substrate is set by the difference in pressure $\Delta P = p_L - p_c$ measured between the wet substrate–liquid interface $[z = h_s(r,t)]$ and the wet substrate–dry substrate interface $[z = h_l(r,t)]$. The capillary pressure scales with the total surface area of the solid–liquid interface per unit volume[23] in the porous substrate while p_L scales with the curvature of the liquid drop. Consequently, $\Delta P \approx -p_c > 0$ characterizes the situation in which the pressure difference across the wet substrate is dictated primarily by capillary suction; we take this to be the case here. This is consistent with the assumption that the typical pore size in the substrate is much smaller than the droplet diameter.

In this setting the Darcy equation (3) implies that large vertical pressure gradients drive a nearly vertical flow. The horizontal flow decouples from the solid and liquid mass balance equations (1) and (2) and we have the following one-dimensional system of equations for the wet substrate:

$$\frac{\partial \phi}{\partial t} + \frac{\partial}{\partial z}(\phi w_s) = 0, \tag{13}$$

$$\frac{\partial \phi}{\partial t} - \frac{\partial}{\partial z}[(1-\phi) w_l] = 0, \tag{14}$$

$$w_l - w_s = -\frac{K(\phi)}{(1-\phi)\mu}\frac{\partial p}{\partial z}, \tag{15}$$

$$0 = -\frac{\partial p}{\partial z} + \frac{\partial \sigma}{\partial z}. \tag{16}$$

These equations are consistent with the one-dimensional models examined by Preziosi *et al.*[22] and by Barry and Aldis[33,47] who additionally considered radial flows in cylindrical and spherical geometries.

Before we discuss boundary conditions for this reduced system of equations we note that Eqs. (13)–(16) can be reduced to a single partial differential equation (PDE) for the solid volume fraction ϕ, as shown by Preziosi *et al.* This is accomplished by subtracting Eq. (14) from Eq. (13) so that $\partial/\partial z[\phi w_s + (1-\phi) w_l] = 0$ and

$$\phi w_s + (1-\phi) w_l = c_0(r,t), \tag{17}$$

where c_0 is an arbitrary function to be determined. Using this result and Eq. (15) we find that

$$w_s = c_0(r,t) + \frac{K(\phi)}{\mu}\frac{\partial p}{\partial z}, \tag{18}$$

$$w_l = c_0(r,t) - \frac{\phi}{1-\phi}\frac{K(\phi)}{\mu}\frac{\partial p}{\partial z}. \tag{19}$$

By the stress equilibrium statement (16) and the constitutive relation $\sigma = \sigma(\phi)$ we note that $\partial p/\partial z = \sigma'(\phi)\partial\phi/\partial z$. Therefore, Eq. (13) can be written as

$$\frac{\partial \phi}{\partial t} + c_0(r,t)\frac{\partial \phi}{\partial z} = -\frac{\partial}{\partial z}\left(\frac{\phi K(\phi)\sigma'(\phi)}{\mu}\frac{\partial \phi}{\partial z}\right) \tag{20}$$

on $h_l(r,t) < z < h_s(r,t)$. Equation (20) is equivalent to Eq. (44) in Preziosi *et al.*[22]

A. Boundary conditions for Region IIa

The boundary conditions applied at the liquid–wet substrate interface $z=h_s(r,t)$ for $0 \leqslant r \leqslant a(t)$ are

$$w_s(h_s^-,t) = \frac{\partial h_s}{\partial t}, \tag{21}$$

$$p(h_s^-,t) = p_A + p_L, \tag{22}$$

$$\sigma(h_s^-,t)=0. \tag{23}$$

The boundary conditions applied at the wet substrate–dry substrate interface $z=h_l(r,t)$ are

$$w_l(h_l^+,t)=\frac{\partial h_l}{\partial t}, \tag{24}$$

$$p(h_l^+,t)=p_A+p_c. \tag{25}$$

An expression for $c_0(r,t)$ can be derived following the arguments in Preziosi *et al.* which we outline below. Evaluating and equating $c_0(r,t)=\phi w_s+(1-\phi)w_l$ on both sides of the wet–dry substrate interface gives

$$\begin{aligned} c_0(r,t) &= \phi(h_l^+)w_s(h_l^+)+[1-\phi(h_l^+)]w_l(h_l^+) \\ &= [1-\phi_0]w_l(h_l^+), \end{aligned} \tag{26}$$

where $\phi(h_l^-)=\phi_0$, $w_s(h_l^-)=0$ (the dry substrate is rigid) and we have assumed that $w_l(h_l^-)=w_l(h_l^+)$. Another way of viewing the latter assumption is that $w_v(h_l^-)=w_l(h_l^+)$ where w_v is the vertical component of the vapor velocity in the dry substrate. From the above result we obtain their Eq. (28):

$$w_s(h_l^+)=\frac{\phi(h_l^+)-\phi_0}{\phi(h_l^+)}w_l(h_l^+)=\frac{\phi(h_l^+)-\phi_0}{\phi(h_l^+)(1-\phi_0)}c_0(r,t). \tag{27}$$

Now Eqs. (18) and (27) imply that

$$c_0(r,t)=-\frac{(1-\phi_0)}{\phi_0}\frac{\phi K(\phi)\sigma'(\phi)}{(1-\phi)\mu}\left.\frac{\partial\phi}{\partial z}\right|^{h_l^+}. \tag{28}$$

Equation (20) along with boundary conditions (21)–(25) and the expression for $c_0(r,t)$ in Eq. (28) represents a closed system. To see this, note that Eq. (16) along with the pressure and stress boundary conditions at $z=h_s(r,t)$ imply that the pressure throughout Region IIa is given by

$$p=\sigma(\phi)+p_A+p_L. \tag{29}$$

Therefore, the pressure boundary condition at $z=h_l(r,t)$ can be written as $\sigma(\phi(h_l^+,t))=p_c-p_L=-\Delta P$. Consequently, the problem can be reduced to solving Eq. (20) subject to the boundary conditions $\sigma(\phi(h_s^-,t))=0$ and $\sigma(\phi(h_l^+,t))=-\Delta P$. Note that we can interpret these two equations as Dirichlet boundary conditions on ϕ once the form of $\sigma(\phi)$ is specified. That is, we can define ϕ_l and ϕ_s implicitly through the conditions

$$\sigma(\phi_s)\equiv 0, \quad \sigma(\phi_l)\equiv -\Delta P. \tag{30}$$

The interface positions are found using Eqs. (21) and (24) which we write as

$$\frac{\partial h_s}{\partial t}=c_0(r,t)+\frac{K(\phi)\sigma'(\phi)}{\mu}\left.\frac{\partial\phi}{\partial z}\right|^{h_s^-}, \tag{31}$$

$$\frac{\partial h_l}{\partial t}=c_0(r,t)-\frac{\phi K(\phi)\sigma'(\phi)}{(1-\phi)\mu}\left.\frac{\partial\phi}{\partial z}\right|^{h_l^+}. \tag{32}$$

The second condition listed in (30) implies a relationship between ϕ_l and ΔP. One may argue that the value of ϕ_l should be determined by local physics near the penetrating front and should be independent of quantities such as p_L. We shall interpret this condition as the definition of ϕ_l [see Eq. (43) which includes our assumed form for $\sigma(\phi)$] and treat ϕ_l as an input parameter whose dependence on the problem we investigate. We shall find that the value of ϕ_l, and in particular its value relative to the dry substrate solid fraction ϕ_0, is an indicator of the state of deformation in the final wet substrate configuration.

B. Boundary conditions for Region IIb

As mentioned above we consider two models for the substrate in this region.

In Case A, we simply freeze the evolution; that is, there is no additional evolution or substrate deformation in the region $a<r<R$. Here the deformed substrate shape is determined by tracking the coordinates $[a(t),h_s(a(t),t)]$ for the upper substrate position and the coordinates $[a(t),h_l(a(t),t)]$ for the lower substrate position. This situation gives a characterization of the deformation that occurs only during the actual imbibition process. This model may reflect results of more sophisticated models that include evaporation or other drying effects that may retard the motion of the wet substrate–air interface.

In Case B, the substrate deformation and liquid penetration continues in response to solid fraction (or deformation) gradients in the wet substrate. Recall that in Region IIa the pressure inside the wet substrate region is given by Eq. (29). Along the bottom boundary $z=h_l$ in Region IIb we have the same condition on pressure ($p=p_A+p_c$) as for the boundary $z=h_l$ in Region IIa. We additionally assume that the same solid fraction ϕ_l is maintained in this region as well. As a result, the pressure throughout the wet substrate, including both Region IIa and Region IIb is given by Eq. (29). Other conditions that remain unchanged for Region IIb are the kinematic conditions (21) and (24) as well as the expression for c_0 in Eq. (28). A new boundary condition is applied at the interface $z=h_s(r,t)$ which states that the vertical fluid velocity is equal to the vertical solid velocity, $w_l=w_s$. Owing to Darcy's equation and the stress equilibrium balance, this condition can be rewritten as $\partial\phi/\partial z=0$ at this boundary. Physically, this boundary condition states that the wet substrate–air interface neither dries out (drying out means $w_s>w_l$) nor forms "puddles" (puddles form if $w_l>w_s$). Note that in general $w_s\neq 0$ so the wet substrate–air interface continues to evolve in response to solid fraction (or deformation) gradients in the wet substrate. This boundary is not assumed to be stress free ($\sigma\neq 0$ in general) and the pressure at the interface is known via Eq. (29) once the solid fraction ϕ is obtained by solving Eq. (20) subject to the given boundary conditions.

C. Similarity formulation for Region IIa

Equation (20) subject to the boundary conditions for Region IIa described above admits a solution in terms of the similarity variable

$$\eta = \frac{z}{2\sqrt{Dt}}, \tag{33}$$

where D has units of length squared per unit time and will be specified below. Additionally, the interface positions are planar and can be expressed as

$$h_s(t) = 2\lambda_s\sqrt{Dt}, \quad h_l(t) = 2\lambda_l\sqrt{Dt}. \tag{34}$$

A standard transformation of Eq. (20) leads to the ordinary differential equation (ODE):

$$2\eta\frac{d\phi}{d\eta} + \frac{(1-\phi_0)}{\phi_0}\left[\frac{\phi K(\phi)\sigma'(\phi)}{(1-\phi)\mu D}\frac{d\phi}{d\eta}\right]_{\lambda_l^+}\frac{d\phi}{d\eta} = \frac{d}{d\eta}\left[\frac{\phi K(\phi)\sigma'(\phi)}{\mu D}\frac{d\phi}{d\eta}\right]. \tag{35}$$

Note that the coefficient of the second term on the left-hand side of this equation is a constant. This equation is subject to the boundary conditions $\sigma(\phi(\lambda_s^-))=0$ and $\sigma(\phi(\lambda_l^+))=-\Delta P$. The values of λ_s and λ_l are determined by solving the equations

$$\lambda_s = \frac{1}{2}\left\{-\frac{(1-\phi_0)}{\phi_0}\left[\frac{\phi K(\phi)\sigma'(\phi)}{(1-\phi)\mu D}\frac{d\phi}{d\eta}\right]_{\lambda_l^+} + \left[\frac{K(\phi)\sigma'(\phi)}{\mu D}\frac{d\phi}{d\eta}\right]_{\lambda_s^-}\right\}, \tag{36}$$

$$\lambda_l = -\frac{1}{2}\left[\frac{\phi K(\phi)\sigma'(\phi)}{\phi_0(1-\phi)\mu D}\frac{d\phi}{d\eta}\right]_{\lambda_l^+}. \tag{37}$$

Equations (35)–(37) can be solved numerically once appropriate expressions for $K(\phi)$ and $\sigma(\phi)$ are specified. Preziosi *et al.*[22] have examined solutions of this equation for empirically determined values of $\sigma(\phi)$ and $K(\phi)$ corresponding to a polyurethane sponge in experiments of Sommer and Mortensen.[21]

Our objective for this model is in terms of a qualitative characterization of possible behavior rather than a quantitative analysis for specific materials. Consequently, in the calculations that follow we shall make special choices for the functions $K(\phi)$ and $\sigma(\phi)$ which are consistent with physically realistic trends but at the same time allow for a nearly analytical solution to be obtained. In particular, suppose that

$$K(\phi) = \frac{K_0}{\phi}, \quad \sigma(\phi) = m(\phi_r - \phi), \tag{38}$$

where $K_0>0$ and $m>0$ so that $\sigma'(\phi)=-m<0$. This permeability function is inversely proportional to the solid fraction (regions of higher solid fraction correspond to lower permeability and regions of lower solid fraction corresponds to higher permeability). We expect this to be a reasonable model when the solid fraction is not very near the extreme values of 0 or 1. The stress function is zero when the solid fraction is at a "relaxed" value of ϕ_r (which we take to be a prescribed constant). The sign choice for m is consistent with that used in Preziosi *et al.* Note that from Eq. (29) we then have $p=m(\phi_r-\phi)+p_A+p_L$ so that pressure gradients oppose solid fraction gradients; increases in the liquid pressure lead to reductions in the solid fraction. Additionally, we choose $D=K_0m/\mu$ and note that

$$\frac{\phi K(\phi)\sigma'(\phi)}{\mu D} = -1. \tag{39}$$

For a typical pore size $l=1$ μm and a typical surface tension $\gamma=30$ mN m^{-1} (e.g., Clarke *et al.*) we can estimate the capillary pressure $|p_c|\approx\gamma/l\approx10^4$ Pa. Then $m\approx|\Delta\sigma/\Delta\phi| \approx|p_c/\Delta\phi|\approx10^4/0.2$ Pa$\approx10^5$ Pa. Also, for the system considered by Preziosi *et al.* an estimate for K_0 can be obtained by their figure 2; $K_0=\phi_rK(\phi_r)\approx(0.1)10^{-11}$ m$^2\approx10^{-12}$ m^2. Using $\mu\approx10^{-3}$ Pa s gives $D\approx10^{-4}$ m^2/s.

Now Eq. (35) reduces to

$$-2(\eta-B)\frac{d\phi}{d\eta} = \frac{d^2\phi}{d\eta^2}, \tag{40}$$

where B is a constant defined by

$$B = \frac{(1-\phi_0)}{2\phi_0}\left[\frac{1}{1-\phi}\frac{d\phi}{d\eta}\right]_{\lambda_l^+}. \tag{41}$$

Equation (40) is subject to the boundary conditions

$$\phi = \phi_r, \quad \text{at } \eta=\lambda_s, \tag{42}$$

$$\phi = \phi_l \equiv \phi_r + \frac{\Delta P}{m}, \quad \text{at } \eta=\lambda_l. \tag{43}$$

The values of λ_s and λ_l simplify in Eqs. (36) and (37) and are given by

$$\lambda_l = \frac{1}{2\phi_0}\left[\frac{1}{1-\phi}\frac{d\phi}{d\eta}\right]_{\lambda_l^+}, \tag{44}$$

$$\lambda_s = (1-\phi_0)\lambda_l - \frac{1}{2}\left[\frac{1}{\phi}\frac{d\phi}{d\eta}\right]_{\lambda_s^-}. \tag{45}$$

The solution to Eq. (40) can be written down in terms of error functions as follows:

$$\phi(\eta) = \frac{\mathrm{erf}(\lambda_s-B)-\mathrm{erf}(\eta-B)}{\mathrm{erf}(\lambda_s-B)-\mathrm{erf}(\lambda_l-B)}(\phi_l-\phi_r)+\phi_r, \tag{46}$$

where

$$B = (1-\phi_0)\lambda_l, \tag{47}$$

$$\lambda_s = \frac{(\phi_l-\phi_r)}{\sqrt{\pi}[\mathrm{erf}(\lambda_s-B)-\mathrm{erf}(\lambda_l-B)]} \times\left\{\frac{1}{\phi_r}\exp[-(\lambda_s-B)^2] - \frac{(1-\phi_0)}{\phi_0(1-\phi_l)}\exp[-(\lambda_l-B)^2]\right\}, \tag{48}$$

$$\lambda_l = -\frac{(\phi_l-\phi_r)\exp[-(\lambda_l-B)^2]}{\phi_0(1-\phi_l)\sqrt{\pi}[\mathrm{erf}(\lambda_s-B)-\mathrm{erf}(\lambda_l-B)]}. \tag{49}$$

The solution to the problem is given by Eq. (46) once Eqs. (47)–(49) are solved to obtain B, λ_s, and λ_l. We note

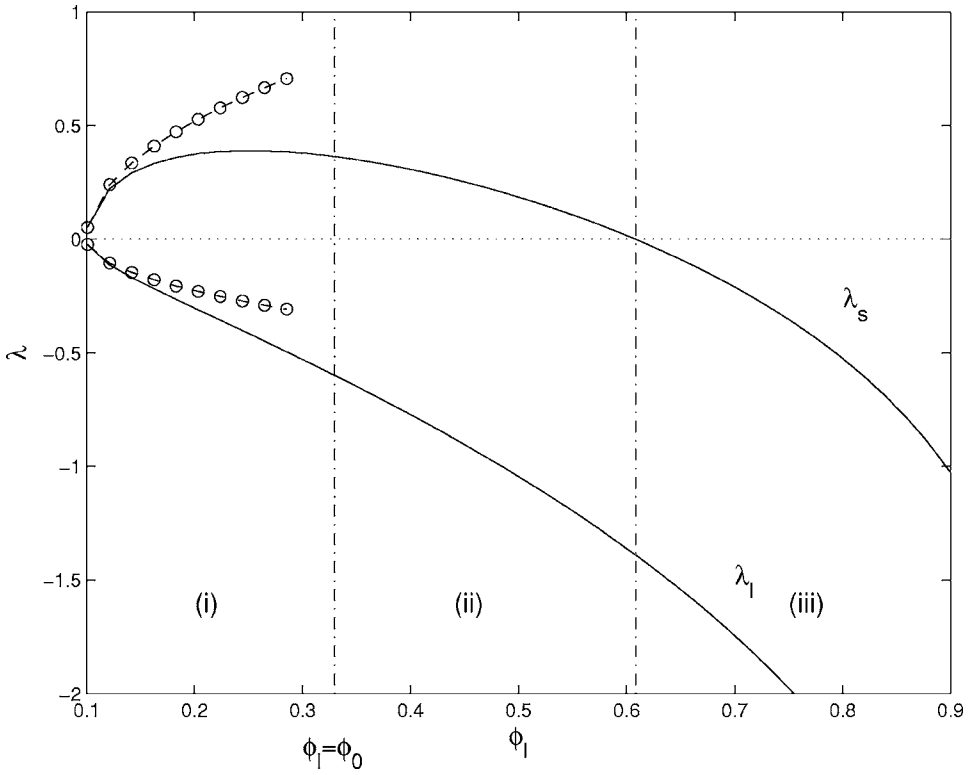

FIG. 2. This figure shows λ_s and λ_l as functions of ϕ_l for $\phi_0=0.33$ and $\phi_r=0.1$. The solid lines are numerical solutions to Eqs. (47)–(49). The dashed lines with open circles indicate the asymptotic solutions given in Eq. (50). This figure, along with results described in the text, reveal three key regimes possible in the one-dimensional imbibition and substrate deformation: (i) swelling during imbibition and an enlarged substrate in equilibrium (here $\lambda_s>0$, $\lambda_l<0$ and $h_s^\infty>0$, $h_l^\infty<0$), (ii) swelling during imbibition but relaxation to a compacted substrate in equilibrium (here $\lambda_s>0$, $\lambda_l<0$ and $h_s^\infty<0$, $h_l^\infty<0$), and (iii) shrinkage during imbibition and a compacted substrate in equilibrium (here $\lambda_s<0$, $\lambda_l<0$ and $h_s^\infty<0$, $h_l^\infty<0$). Note that h_s^∞ and h_l^∞ are defined in Eqs. (69).

that if (B,λ_l,λ_s) is a solution so is $(-B,-\lambda_l,-\lambda_s)$. For the imbibition process we require $\lambda_l<0$ so that liquid front penetrates down into the substrate. In an effort to understand the solutions of Eqs. (47)–(49) we examine two limiting cases in which analytical solutions may be identified. If $\phi_l=\phi_r+\epsilon$ where ϵ is a small positive number and $\phi_0-\phi_r=O(1)$, then

$$\lambda_s \sim \left(\frac{\phi_0-\phi_r}{\phi_0}\right)\left[\frac{1}{2\phi_r(1-\phi_r)}\right]^{1/2}\epsilon^{1/2},$$
$$\lambda_l \sim -\frac{\phi_r}{\phi_0}\left[\frac{1}{2\phi_r(1-\phi_r)}\right]^{1/2}\epsilon^{1/2}, \tag{50}$$

with $B\sim(1-\phi_0)\lambda_l$. If $\phi_l=\phi_0=\phi_r+\epsilon$, then a modified asymptotic result applies

$$\lambda_s \sim \frac{1}{2\phi_r}\left[\frac{1}{2\phi_r(1-\phi_r)}\right]^{1/2}\epsilon^{3/2},$$
$$\lambda_l \sim -\left[\frac{1}{2\phi_r(1-\phi_r)}\right]^{1/2}\epsilon^{1/2}, \tag{51}$$

with $B\sim(1-\phi_r)\lambda_l$.

Figure 2 shows values of λ_s and λ_l plotted as functions of ϕ_l for $\phi_0=0.33$ and $\phi_r=0.1$. The solid lines are the numerical solutions to Eqs. (47)–(49) while the dashed lines with open circles indicate the asymptotic results given in Eq. (50). This figure indicates three important solution regimes possible for one-dimensional imbibition and substrate deformation which we shall describe in more detail below when we examine the imbibition and deformation of a finite volume of fluid. We can note at this point, however, that it is possible for $\lambda_s>0$ (so that the substrate interface moves upward—i.e., the substrate swells during imbibition) and also for $\lambda_s<0$ (so that the substrate interface moves downward—i.e., the substrate shrinks during imbibition). A third related scenario emerges when we discuss equilibrium configurations of the wet-substrate for finite fluid volumes.

Figure 3 shows values of λ_s and λ_l plotted as functions of ϕ_l for the case $\phi_0=\phi_l$ with $\phi_r=0.1$. The solid lines are the numerical solutions to Eqs. (47)–(49) while the dashed lines with open circles indicate the asymptotic results given in Eq. (51). In contrast to the case where $\phi_l\neq\phi_0$, here the dynamics are limited to the case in which $\lambda_s>0$ and $\lambda_l<0$. Note that we consider only $\phi_l>\phi_r$ since when $\phi_l=\phi_r$ we find that $\lambda_s=\lambda_l$ which has no imbibition or substrate deformation. In this model, pressure gradients (e.g., due to capillarity and leading to imbibition) necessarily accompany solid fraction gradients (leading to substrate deformation). This tight coupling between pressure and deformation can be observed in Eq. (29); one does not exist in this model without the other.

In the cases we discuss below, we shall examine primarily three sets of input values which fix values of ϕ_0 and ϕ_r and allow ϕ_l to vary. These three data sets are shown in Table I.

D. Model and numerical solution for Region IIb

Our solution of the droplet evolution in this region is based on the following observation. Suppose that we fix a value of $r<R_0$. We define $t_I(r)$ as the time at which the column (actually the annulus in this radially symmetric geometry) of fluid at radius r is completely imbibed by the substrate. So for $t<t_I(r)$ the wet substrate at r evolves with the description for Region IIa and for $t>t_I(r)$ the wet substrate at r evolves with the description for Region IIb. Overall, then, the region at radius r evolves and follows that of a

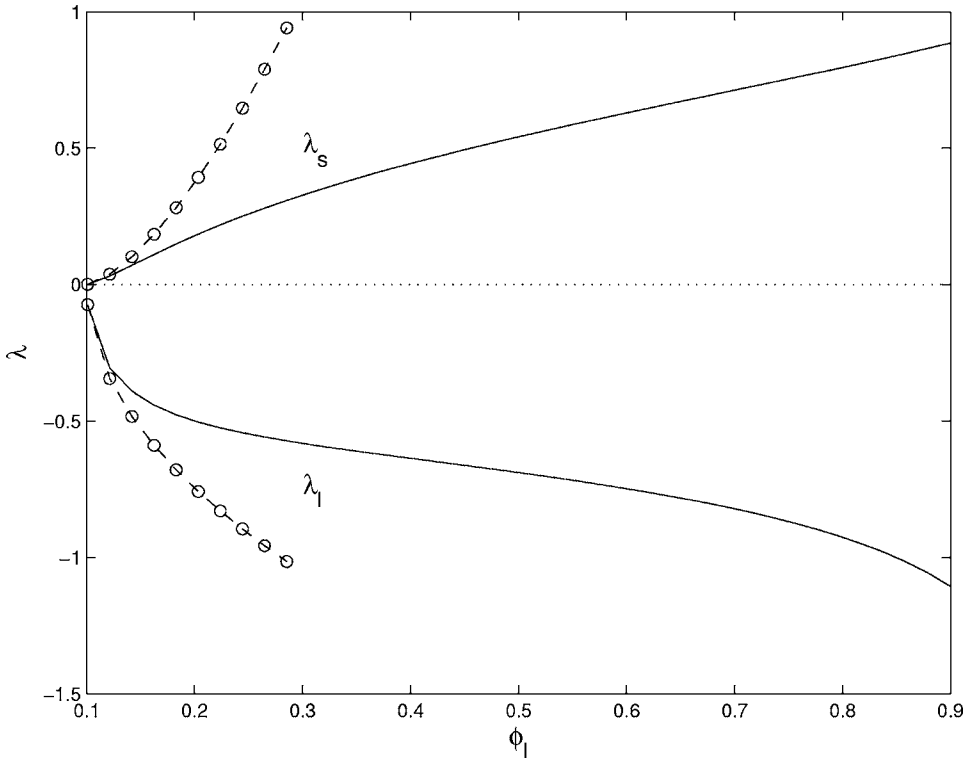

FIG. 3. This figure shows λ_s and λ_l as functions of ϕ_l for the case $\phi_0=\phi_l$ with $\phi_r=0.1$. The solid lines are numerical solutions to Eqs. (47)–(49). The dashed lines with open circles indicate the asymptotic solutions given in Eqs. (51).

one-dimensional imbibition and deformation process with a finite volume supply. In the following discussion we outline a one-dimensional imbibition and deformation process with a finite volume and then describe how it can be adapted for the axisymmetric droplet geometry.

For $t<t_I$ the fluid is available from the supply (i.e., the droplet), the governing equations and boundary conditions are those of Region IIa and so we apply the similarity solution described in the previous section.

After the fluid is completely imbibed, $t>t_I$, we model the evolution of the system with the same equation (20) in the wet porous substrate but with boundary conditions as described for Region IIb. The initial conditions applied to the second stage of the problem at $t=t_I$ correspond to the ending conditions of the first stage. So here we solve Eq. (20) subject to the boundary condition $\phi=\phi_l$ at $z=h_l$ and $\partial\phi/\partial z=0$ at $z=h_s$. The kinematic condition at the interface $z=h_l(t)$ is expressed as

TABLE I. This table shows computed values of B, λ_s, and λ_l from the similarity solution for three different sets of parameter values for ϕ_0, ϕ_l, and ϕ_r.

	Set 1	Set 2	Set 3
ϕ_0	0.33	0.33	0.33
ϕ_l	0.20	0.33	0.50
ϕ_r	0.10	0.10	0.10
B	−0.2029	−0.4015	−0.6995
λ_s	0.3752	0.3646	0.1860
λ_l	−0.3028	−0.5993	−1.0440

$$\frac{dh_l}{dt}=-\frac{1}{\phi_0}\left[\frac{\phi K(\phi)\sigma'(\phi)}{(1-\phi)\mu}\frac{\partial\phi}{\partial z}\right]_{h_l^+}. \tag{52}$$

At the upper boundary, we find that $dh_s/dt=c_0$ or

$$\frac{dh_s}{dt}=(1-\phi_0)\frac{dh_l}{dt}. \tag{53}$$

As before we consider the case where $K(\phi)=K_0/\phi$ and $\sigma(\phi)=m(\phi_r-\phi)$ which leads to the equation

$$\frac{\partial\phi}{\partial t}+D\frac{(1-\phi_0)}{\phi_0}\left[\frac{1}{(1-\phi)}\frac{\partial\phi}{\partial z}\right]_{h_l^+}\frac{\partial\phi}{\partial z}=D\frac{\partial^2\phi}{\partial z^2}, \tag{54}$$

subject to the boundary conditions

$$\phi=\phi_l, \quad \text{at } z=h_l(t), \tag{55}$$

$$\frac{\partial\phi}{\partial z}=0, \quad \text{at } z=h_s(t), \tag{56}$$

and

$$\frac{dh_l}{dt}=\frac{D}{\phi_0}\left[\frac{1}{(1-\phi)}\frac{\partial\phi}{\partial z}\right]_{h_l^+}, \tag{57}$$

$$\frac{dh_s}{dt}=(1-\phi_0)\frac{dh_l}{dt}, \tag{58}$$

where $D=K_0m/\mu$. For initial conditions we use the similarity solution for ϕ, h_l, and h_s given by Eqs. (46) and (34) for a value of time $t=t_I$ at which the liquid supply is depleted. For the strictly one-dimensional problem of imbibition of a finite volume of fluid and the corresponding substrate deformation,

an analytical expression related to the initial volume of fluid can be found for t_I (see Appendix A). For the droplet problem this time is a function of radial position $t_I = t_I(r)$ and is dependent on the particular model used to describe the liquid droplet evolution. Below we describe a solution to the finite liquid volume problem and how it can be used for the droplet problem.

1. Dimensionless system and solution

The system defined by Eqs. (54)–(58) plus initial conditions requires numerical solution. In the droplet problem we have initial times that depend on the radial position $t_I(r)$ and so we will need the solution for a range of t_I values and corresponding ranges of values for $h_s(t_I)$ and $h_l(t_I)$. We find that by first nondimensionalizing this system, a single numerical solution can be used to deduce the solution for all initial conditions of interest.

We introduce dimensionless quantities (denoted by overbars) into the above system (54)–(58):

$$\bar{z} = \frac{z - h_l^I}{\Delta h}, \quad \bar{t} = \frac{D(t - t_I)}{(\Delta h)^2},$$
$$\bar{h}_l = \frac{h_l - h_l^I}{\Delta h}, \quad \bar{h}_s = \frac{h_s - h_l^I}{\Delta h}, \tag{59}$$

where h_l^I is the initial value of $h_l(t)$, h_s^I is the initial value of $h_s(t)$ and $\Delta h = h_s^I - h_l^I$. Note that Δh is the thickness of the deformed wet substrate when the supply of fluid above is depleted (complete imbibition).

In terms of these dimensionless quantities the governing equations are

$$\frac{\partial \phi}{\partial \bar{t}} + \frac{1 - \phi_0}{\phi_0}\left[\frac{1}{(1-\phi)}\frac{\partial \phi}{\partial \bar{z}}\right]_{\bar{z}=\bar{h}_l^+}\frac{\partial \phi}{\partial \bar{z}} = \frac{\partial^2 \phi}{\partial \bar{z}^2}, \tag{60}$$

subject to the boundary conditions

$$\phi = \phi_l, \quad \text{at } \bar{z} = \bar{h}_l(\bar{t}), \tag{61}$$

$$\frac{\partial \phi}{\partial \bar{z}} = 0, \quad \text{at } \bar{z} = \bar{h}_s(\bar{t}), \tag{62}$$

and

$$\frac{d\bar{h}_l}{d\bar{t}} = \frac{1}{\phi_0}\left[\frac{1}{(1-\phi)}\frac{\partial \phi}{\partial \bar{z}}\right]_{\bar{z}=\bar{h}_l^+}, \tag{63}$$

$$\frac{d\bar{h}_s}{d\bar{t}} = (1 - \phi_0)\frac{d\bar{h}_l}{d\bar{t}}. \tag{64}$$

The initial conditions for the interface positions are

$$\bar{h}_l(\bar{t} = 0) = 0, \tag{65}$$

$$\bar{h}_s(\bar{t} = 0) = 1. \tag{66}$$

The initial condition for ϕ can be derived by first noting that $\phi(z, t_I) = \phi(z/2\sqrt{Dt_I})$ from the similarity solution where

$$\frac{z}{2\sqrt{Dt_I}} = \frac{h_l^I + \bar{z}(h_s^I - h_l^I)}{2\sqrt{Dt_I}} = \frac{2\lambda_l\sqrt{Dt_I} + 2\bar{z}(\lambda_s - \lambda_l)2\sqrt{Dt_I}}{2\sqrt{Dt_I}} = \lambda_l + \bar{z}(\lambda_s - \lambda_l). \tag{67}$$

Therefore, the initial condition for ϕ in dimensionless form is

$$\phi(\bar{z}, \bar{t} = 0) = \phi(\lambda_l + \bar{z}(\lambda_s - \lambda_l)), \tag{68}$$

evaluated using the similarity solution (46).

We have solved numerically the free boundary problem (60)–(64) subject to initial conditions (65), (66), and (68). The numerical procedure uses an implicit finite difference scheme with second-order accurate differences in space and first order in time (based on a similar implementation described in Anderson, McLaughlin and Miller[48]). The resulting nonlinear system of equations was solved using the nonlinear solver hybrd.f [which is based on a modification of the Powell hybrid method, and is available in the MINPACK package at NETLIB (www.netlib.org)].

Before showing the numerical results we point out a simple calculation based on mass conservation applied to the liquid and solid phases that will help interpret the results. If one takes as the long-time behavior of the system the state of uniform solid fraction ϕ_l throughout the wet substrate region then one obtains the following two formulas for the upper and lower wet substrate interface positions:

$$h_s^\infty = \left(1 - \frac{\phi_l}{\phi_0}\right)\frac{V_0}{1 - \phi_l}, \quad h_l^\infty = -\frac{\phi_l}{\phi_0}\frac{V_0}{1 - \phi_l}, \tag{69}$$

where V_0 is the initial volume of fluid per unit area (i.e., the initial height of the liquid column in this one-dimensional setting). We see that while $h_l^\infty < 0$ for all physically relevant parameter values, h_s^∞ may be positive (when $\phi_l < \phi_0$), negative (when $\phi_l > \phi_0$) or zero (when $\phi_l = \phi_0$). With these results we can make a full interpretation of the three regimes identified in Fig. 2. In regime (i) where $\phi_l < \phi_0$ swelling occurs during imbibition and the equilibrium configuration corresponds to an enlarged substrate [here $\lambda_s > 0$, $\lambda_l < 0$ and $h_s^\infty > 0$, $h_l^\infty < 0$]. In regime (ii) where $\phi_l > \phi_0$ (and less than the critical value for which λ_s becomes negative), swelling occurs during imbibition but the equilibrium configuration corresponds to a compacted substrate [here $\lambda_s > 0$, $\lambda_l < 0$ and $h_s^\infty < 0$, $h_l^\infty < 0$]. In regime (iii) where ϕ_l is greater than the critical value for which λ_s becomes negative, shrinkage occurs during imbibition and the equilibrium configuration corresponds to a compacted substrate [here $\lambda_s < 0$, $\lambda_l < 0$ and $h_s^\infty < 0$, $h_l^\infty < 0$]. Note that an undeformed equilibrium configuration for the wet substrate (where $h_s^\infty = 0$) occurs at a different value of ϕ_l than the situation in which the substrate interface does not move *during* imbibition (i.e., where $\lambda_s = 0$). Consequently, it is clear that this model does not include imbibition into a rigid substrate as a special case since that scenario has a motionless substrate interface and an undeformed equilibrium configuration all at a fixed value of ϕ. We observe these long-time situations in the numerical solu-

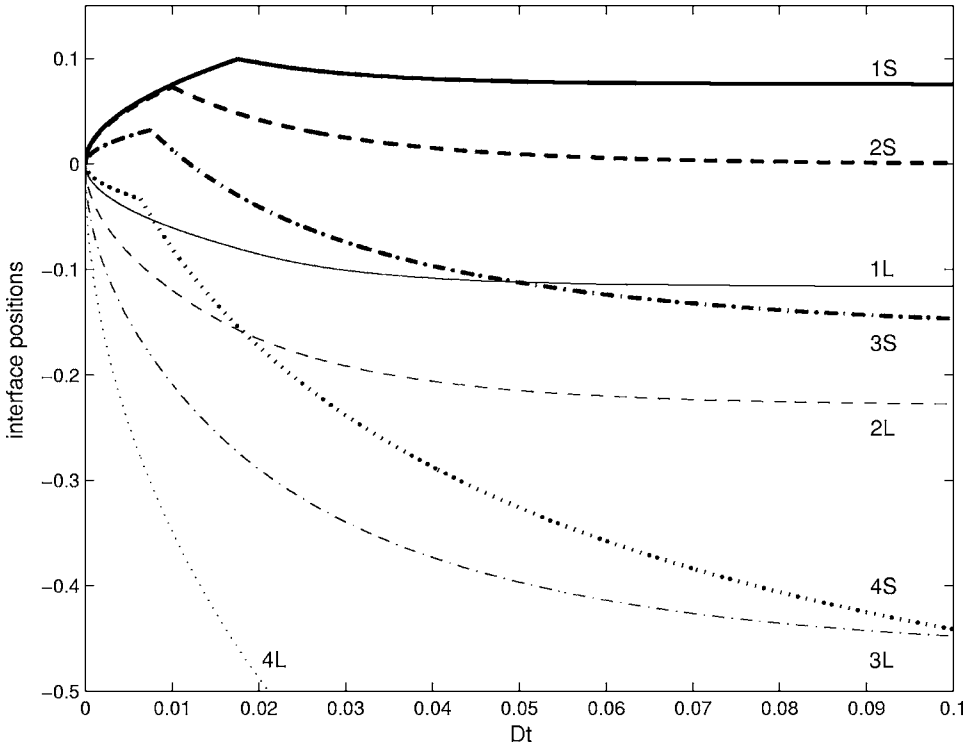

FIG. 4. This figure shows the evolution of the interface positions $h_s(t)$ (curves 1S, 2S, 3S, and 4S) and $h_l(t)$ (curves 1L, 2L, 3L, and 4L) for four cases of a finite volume of fluid penetration. All curves have $\phi_r=0.1$ and $\phi_0=0.33$. Curves 1S and 1L have $\phi_l=0.2$, Curves 2S and 2L have $\phi_l=\phi_0=0.33$, Curves 3S and 3L have $\phi_l=0.5$ and Curves 4S and 4L have $\phi_l=0.7$. See the text for a description of these results. Computations for the ϕ field in the second phase of evolution were done using $NX=400$ (number of grid points in space) and $NT=800$ (number of grid points in time). A value of $V_0=0.1532$ was used in each case.

tions shown below and in the droplet solutions to follow.

Figure 4 shows the evolution of the interface positions $h_s(t)$ (bold curves) and $h_l(t)$ (normal curves) for four cases of one-dimensional penetration and substrate deformation for a finite volume of fluid. For each set of parameters, two phases of evolution occur. During the first phase, the solution is given by the similarity solution (see Sec. III C). Here h_l evolves downward (since $\lambda_l<0$ in all cases) into the initially dry substrate and h_s moves upward when $\lambda_s>0$ and downward when $\lambda_s<0$ (see Fig. 2). When the volume of liquid above the substrate is depleted [at time Dt_1 in Eq. (A5) where the curves for $h_s(t)$ have a discontinuous derivative] further evolution of the wet substrate region is described by the solution to Eqs. (60)–(64) with the similarity solution at t_1 as the initial condition. Here $h_s(t)$ relaxes downward while $h_l(t)$ continues further penetration at a reduced rate. The long term evolution is toward a state in which the solid fraction in the wet substrate has a uniform value ϕ_l. When $\phi_l<\phi_0$ the result is a wet substrate that is expanded from its initial configuration (see Curve 1S). When $\phi_l=\phi_0$ the result is that the substrate relaxes back to an undeformed state (see Curve 2S). When $\phi_l>\phi_0$ the result is a wet substrate that is contracted relative to its initial configuration (see Curves 3S and 4S). A notable difference between curves 3S and 4S is that while they both result in a contracted substrate, the evolution shown in Curve 3S corresponds initially to expansion since $\lambda_s>0$ in that case. The final equilibrium values of h_s and h_l agree with the formulas given in Eq. (69).

This model shows that the initial deformation of the substrate during imbibition is reversed and the long time equilibrium state, which has uniform pressure, stress and solid fraction, is determined by size of ϕ_l relative to ϕ_0. If $\phi_l<\phi_0$ then the substrate will ultimately swell. If $\phi_l=\phi_0$ then the substrate will eventually relax to an undeformed state. If $\phi_l>\phi_0$ then the substrate will ultimately shrink (in this case there may initially be swelling if $\lambda_s>0$). As described below, we show how this behavior appears in the droplet geometry.

IV. AXISYMMETRIC DROPLET SOLUTIONS

We now adapt the above solutions for 1D imbibition and substrate deformation to the axisymmetric droplet problem. We examine only the cases where $K(\phi)=K_0/\phi$ and $\sigma(\phi)=m(\phi_r-\phi)$. The models described below are quasi-two-dimensional in that at each value of r a one-dimensional problem is solved while the interface positions are represented by height functions that vary in space (radial coordinate r) and time.

We examine three different models for the liquid droplet dynamics:

- **Model 1:** Here we require that the contact angle in the liquid is constant in time (e.g., see Denesuk *et al.*[45,46]).
- **Model 2:** Here the liquid droplet shape has curvature which is constant in space and time—this corresponds to the "Central Region" solution identified by Davis and Hocking.[7]
- **Model 3:** Here we impose a relation between the contact line speed and the contact angle used by Clarke *et al.*[2] for spreading on a rigid porous substrate.

We also examine two possible descriptions for how the wet substrate evolves. In the interior region where $0\leqslant r\leqslant a(t)$ (Region IIa) the solution for ϕ is given by the similarity solution (46) and the interface positions $z=h_s(t)$ and $z=h_l(t)$ are planar and are given by Eq. (34). In the exterior region where $a(t)<r<R(t)$ (Region IIb) we consider the following two scenarios:

- **Case A:** Here we suppose that wet substrate region in $a(t)<r<R(t)$ not directly under the liquid droplet is "frozen in." In this case, the final shape of the wet substrate region is determined by the locus of points defined by the penetration depth $h_l(t)$ and the liquid contact line $a(t)$ for the penetration boundary profile and by the deformed height $h_s(t)$ and $a(t)$ for the upper substrate boundary profile.
- **Case B:** The wet-substrate in the exterior region here continues to evolve according to the description and numerical solution above in Sec. III D 1.

Accordingly, we obtain results for six models (Models 1A, 1B, 2A, 2B, 3A, 3B).

In all of these cases, the substrate deformation problem is coupled to the dynamics of the liquid droplet. Specifically, the liquid region (Region I) and the wet substrate region (Regions IIa and IIb) are coupled through a mass conservation condition applied at the droplet–substrate interface

$$\begin{aligned}\frac{dV_L}{dt} &= 2\pi(1-\phi)\int_0^a (w_l - w_s) r\, dr \\ &= \pi a^2 \left[-\frac{K(\phi)\sigma'(\phi)}{\mu}\frac{\partial \phi}{\partial z}\right]\Bigg|^{h_s} \\ &= \pi a^2 D \left[\frac{1}{\phi}\frac{\partial \phi}{\partial z}\right]\Bigg|^{h_s} \\ &= \pi a^2 \frac{D}{2\sqrt{Dt}}\left[\frac{1}{\phi}\frac{d\phi}{d\eta}\right]\Bigg|^{\lambda_s}. \end{aligned} \tag{70}$$

We note that the corresponding results given in Clark *et al.*[2] by their Eqs. (6) and (7) should have V on the left-hand sides rather than $\partial V/\partial t$ (private communication with A. Clarke, 2004). We note that in their work, they introduced a function $\tau(r)$ defined as the time at which the pore at radius r begins to fill. That is, if the liquid droplet is spreading, then pores initially not covered by the liquid droplet may become covered at a later time τ; mass transfer from the droplet into the substrate at this location only begins at $t=\tau(r)$ rather than at $t=0$. In the cases we discuss in the present paper, we consider only receding liquid droplets and so our corresponding value of $\tau(r)=0$. Equation (70) applies in our case for $0<r<a(t)$ and so the mass transfer begins at $t=0$ and ends at $t_l(r)$, where $t_l(r)$ is defined as the time at which the pore at radius r stops filling.

A. Model 1A: Constant contact angle

We assume that the liquid droplet on the substrate always maintains the shape of a spherical cap. This implies that the liquid volume $V_L(t)$ at any time t is given by

$$V_L(t) = \frac{\pi a^3}{3\sin^3\theta}[2 - 3\cos\theta + \cos^3\theta]. \tag{71}$$

We additionally assume that the contact angle θ is constant. This allows us to write

$$\frac{dV_L}{dt} = a^2 \frac{da}{dt} g(\theta), \tag{72}$$

where

$$g(\theta) = \frac{\pi}{\sin^3\theta}[2 - 3\cos\theta + \cos^3\theta]. \tag{73}$$

For $\theta \ll 1$, $g(\theta) \sim 3\pi\theta/4$. If we now use Eq. (72) in Eq. (70) we find that

$$\frac{da}{dt} = \frac{\pi}{g(\theta)}\left[\frac{1}{\phi}\frac{d\phi}{d\eta}\right]\Bigg|^{\lambda_s} \frac{D}{2\sqrt{Dt}}, \tag{74}$$

so that using Eq. (45) we obtain

$$a(t) = a_0 + \frac{2\pi\lambda_l}{g(\theta)}\left(1 - \phi_0 - \frac{\lambda_s}{\lambda_l}\right)\sqrt{Dt}, \tag{75}$$

where we note that $\lambda_l<0$ for penetration into the substrate so that $a(t)$ decreases monotonically in time. The droplet disappearance time is

$$t_D = \frac{1}{D}\left[\frac{a_0 g(\theta)}{2\lambda_l \pi(1-\phi_0-\lambda_s/\lambda_l)}\right]^2. \tag{76}$$

We can now combine Eq. (75) with $h_l(t)=2\lambda_l\sqrt{Dt}$ and $h_s(t)=2\lambda_s\sqrt{Dt}$ in Eq. (34), noting that the final wet substrate profiles for Case A are determined by the locus of points defined by the contact line position with $h_s(t)$ for the upper surface and with $h_l(t)$ for the lower surface. We find that the deformed substrate shape can be expressed by simple, *analytical*, expressions:

$$h_l(r) = -\frac{g(\theta)}{\pi(1-\phi_0-\lambda_s/\lambda_l)}[a_0 - r], \tag{77}$$

$$h_s(r) = -\frac{\lambda_s}{\lambda_l}\frac{g(\theta)}{\pi(1-\phi_0-\lambda_s/\lambda_l)}[a_0 - r], \tag{78}$$

for $r \geqslant a(t)$. An example of the time evolution of the imbibition and deformation is shown in Fig. 5. We see that the interior interface positions [for $0 \leqslant r \leqslant a(t)$] are planar and the exterior interface positions [for $a(t) \leqslant r \leqslant R_0$] are part of a conical surface. The final configuration is that of a cone-shaped deformation/penetration profile. Note that these expressions depend on ϕ_l and ϕ_r only through the resulting values of λ_s and λ_l. There is a striking similarity of this solution to the predictions of the shape of a solidified liquid droplet (Anderson, Worster, and Davis[49]) for their case of a constant tri-junction angle. The linear profiles, and hence overall conical shape prediction, are results of both the swelling and penetration fronts having the same functional dependence on time ($\sqrt{t}$) as the contact line position.

As a point of comparison note that if the contact line position is assumed fixed at its initial value a_0 (and the contact angle is free to vary) then one can derive from Eq. (70) that the predicted disappearance time for the droplet is exactly nine times smaller than the one given in Eq. (76). This result, $t_D(\text{fixed angle}) = 9t_D(\text{fixed area})$ is the same result as derived by Denesuk *et al.*[45] for the case of imbibition into a rigid substrate. Also in the case of fixed contact line position,

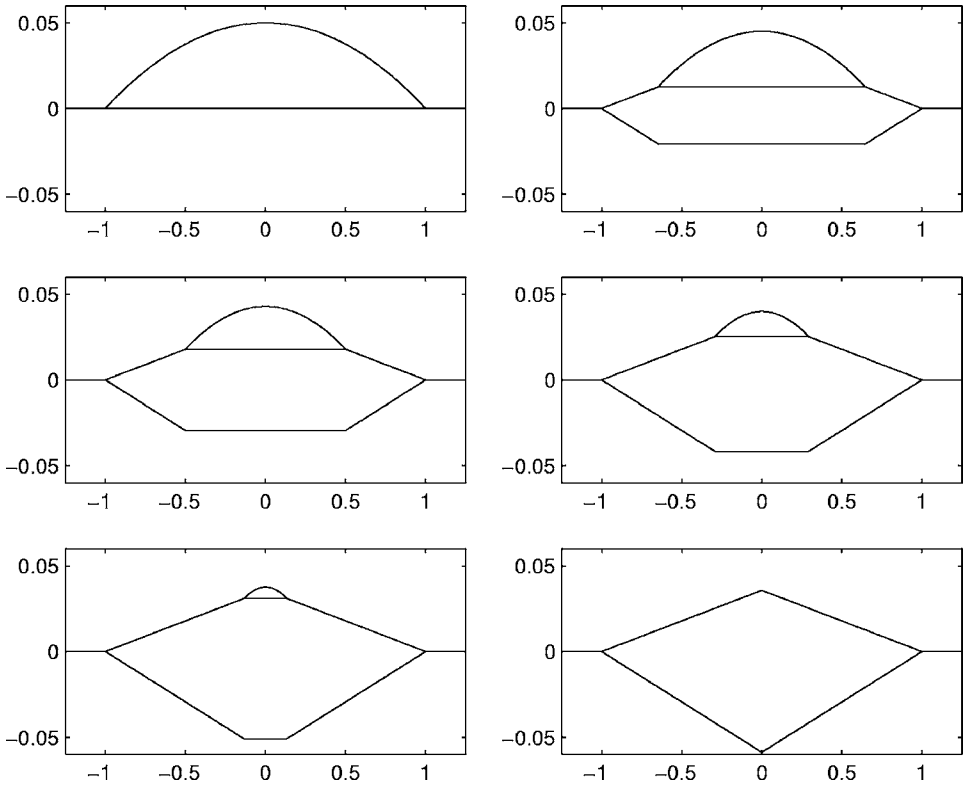

FIG. 5. Model 1A: This figure shows the geometry of the wet substrate region and the liquid droplet for times $t/t_D=0,0.125,0.25,0.5,0.75,1$ (reading left to right first then down), where the time for complete imbibition of the droplet is $t_D=0.0024$. We have used $\theta_0=0.1$ and $a_0=1$ so that $V_0=0.787$. Also $\phi_0=\phi_l=0.33$ and $\phi_r=0.1$.

the final deformed substrate shape is that of a circular disk whose upper surface is elevated from the original substrate height. We observe similar shapes as predictions of the model based on Clarke *et al.* described in Sec. IV E.

In Case A, the solid fraction profiles at a given radial position are frozen in once the liquid droplet has receded past that position. Therefore, in contrast to the results for Case B shown below, the final shapes shown here have nonuniform solid fraction.

B. Model 1B: Constant contact angle

Here we describe the droplet evolution for the case where the wet substrate region continues to evolve after the overlying liquid has been imbibed and the upper surface of the wet substrate exposed to air. As described above for Region IIb, the new boundary condition here requires the fluid and solid velocities to be equal to each other at the wet substrate–air interface. Below we describe the details of the calculations.

Our first objective is to identify the time at which a particular pore at radial position r becomes exposed to air. We set $r=a(t)$ in Eq. (75) and solve the resulting expression for t. The result, which we identify as the time $t_I(r)$ at which fluid at radius r has been completely imbibed by the substrate, is

$$Dt_I(r)=\left[\frac{(r-a_0)g(\theta)}{2\pi\lambda_l(1-\phi_0-\lambda_s/\lambda_l)}\right]^2. \tag{79}$$

For each radial position we can identify the corresponding interface heights $h_s(t_I)$ and $h_l(t_I)$ (i.e., interface heights at the time when the liquid at r is completely imbibed by the substrate). We can determine the evolution of the wet substrate–air interface and the liquid penetration front at a given radial position simply by rescaling our one-dimensional solution described in Sec. III D 1 using the time $t_I(r)$ at which the substrate interface is first exposed to air and the corresponding interface heights $h_s(t_I)$ and $h_l(t_I)$.

In particular, we discretize the radial coordinate on $a(t)<r<R_0$. For each of these radial positions we identify $t_I(r)$ from Eq. (79) and also identify $h_s(t_I)=2\lambda_s\sqrt{Dt_I(r)}$ and $h_l(t_I)=2\lambda_l\sqrt{Dt_I(r)}$. A dimensionless time $\bar{t}=D[t-t_I(r)]/[\Delta h(t_I)]^2$, where $\Delta h(t_I)=2(\lambda_s-\lambda_l)\sqrt{Dt_I(r)}$, is introduced for each radial position r and time t and corresponding values of $\bar{h}_s(\bar{t})$ and $\bar{h}_l(\bar{t})$ are obtained from a precalculated numerical solution of Eqs. (60)–(66). Therefore, for any value of t and any value of $r\in[a(t),R_0]$ we can deduce the appropriate time $\bar{t}$ at which the precalculated solution should be evaluated. Note that since the resulting discrete values of $\bar{t}$ (obtained from discrete values of t and r) used here are not exactly those of the precalculated solution we fit the precalculated numerical solution using cubic splines and then evaluate the resulting interpolation at the required value of $\bar{t}$. The actual interface positions at a given value of r and t that can be plotted are obtained using $h_s(r,t)=2\lambda_s\sqrt{Dt_I(r)}+\bar{h}_s(\bar{t})\Delta h(t_I)$ and $h_l(r,t)=2\lambda_l\sqrt{Dt_I(r)}+\bar{h}_l(\bar{t})\Delta h(t_I)$.

A summary of three main regimes is shown in Fig. 6. The left column of plots has $\phi_l=0.2$, $\phi_0=0.33$ and $\phi_r=0.1$. The center column of plots has $\phi_l=\phi_0=0.33$ and $\phi_r=0.1$. The right column of plots has $\phi_l=0.5$, $\phi_0=0.33$ and $\phi_r=0.1$. A time series is shown in each column with $t/t_D=0.25$, 0.75, 1.5 and 12.0 where $t_D=0.0042$ (column 1), 0.0024 (column 2) and 0.0018 (column 3). The initial configuration for each column is that shown in the upper left plot

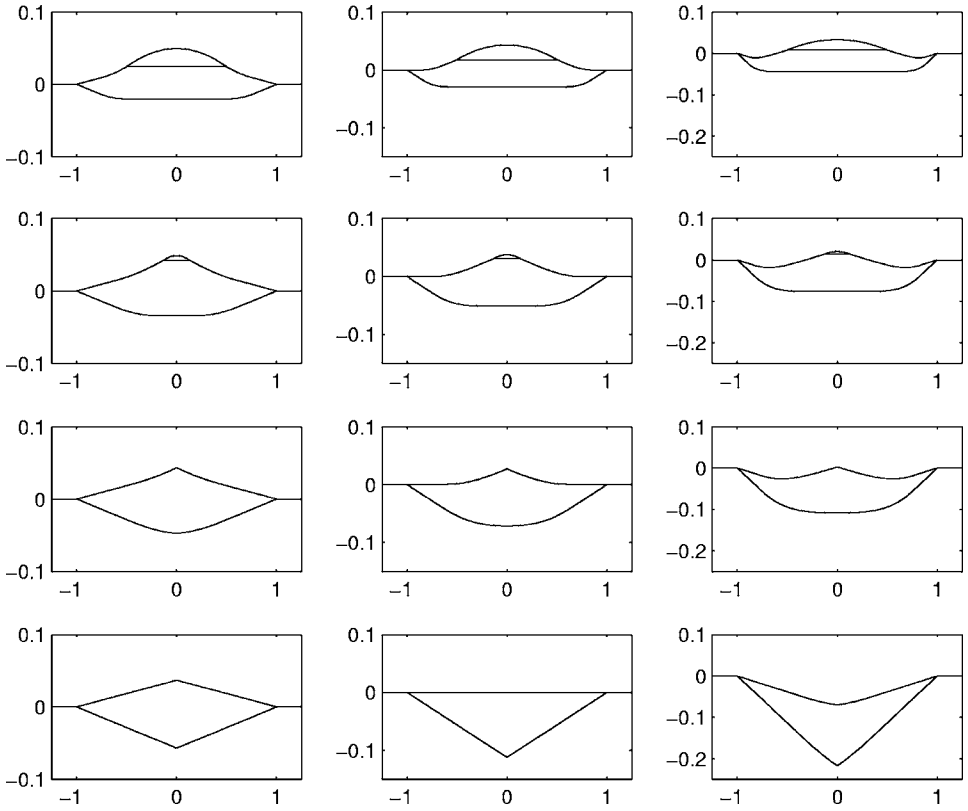

FIG. 6. Model 1B: Three different time series (top to bottom). The left column of plots shows the time series for $\phi_l=0.2$, $\phi_0=0.33$, and $\phi_r=0.1$. The center column of plots has $\phi_l=\phi_0=0.33$ and $\phi_r=0.1$. The right column of plots has $\phi_l=0.5$, $\phi_0=0.33$, and $\phi_r=0.1$. The four rows show the four times $t/t_D=0.25$, 0.75, 1.5, and 12.0 where $t_D=0.0042$ (in column 1), 0.0024 (in column 2) and 0.0018 (in column 3). The initial configuration for each is a parabolic shape as given in the upper left plot of Fig. 5. In each case there is initial swelling of the substrate (since $\lambda_s>0$ here). However, the long time behavior indicates an expanded substrate for $\phi_l<\phi_0$ (left column), an undeformed substrate for $\phi_l=\phi_0$ (center column) and a contracted substrate for $\phi_l>\phi_0$ (right column). In all three cases, the final shape has conical features. Additional parameter values for all cases are $\theta_0=0.1$ and $a_0=1$ so that $V_0=0.787$.

of Fig. 5. In each case there is initial swelling of the substrate (since $\lambda_s>0$ here). However, the long time behavior indicates an expanded substrate for $\phi_l<\phi_0$ (left column), an undeformed substrate for $\phi_l=\phi_0$ (center column) and a contracted substrate for $\phi_l>\phi_0$ (right column). In all three cases, the final shape has conical features. A fourth case (not shown here) includes the situation in which $0>\lambda_s>\lambda_l$ as in the fourth curve in Fig. 2 and behaves similarly to the results in the right column of plots except that the upper substrate surface moves down, rather than up, initially.

C. Model 2A: Davis and Hocking droplet model

This droplet model follows the one discussed in the "Central region" analysis of Davis and Hocking,[7] modified for an axisymmetric geometry. Here the droplet shape has a curvature that is uniform in space and time. In the thin limit, the liquid droplet shape $H(r,t)$ satisfies

$$\frac{\partial}{\partial r}\left[\frac{1}{r}\frac{\partial}{\partial r}\left(r\frac{\partial H}{\partial r}\right)\right]=0. \tag{80}$$

We note that

$$H(r,t)=\frac{2V_0}{\pi a_0^4}(a^2-r^2), \tag{81}$$

satisfies Eq. (80), boundary conditions $H(a,t)=0$ and $\partial H/\partial r(0,t)=0$ and the initial condition

$$H(r,0)=\frac{2V_0}{\pi a_0^4}(a_0^2-r^2), \tag{82}$$

where V_0 is the initial volume and a_0 is the initial contact line position. It follows that the corresponding volume of the liquid droplet is

$$V_L(t)=\frac{V_0}{a_0^4}a^4, \tag{83}$$

and the apparent contact angle $\theta_{APP}=-\partial H/\partial r(a,t)$ is

$$\theta_{APP}=\frac{4V_0}{\pi a_0^4}a. \tag{84}$$

If we now use Eq. (83) in Eq. (70) we find that

$$\frac{d(a^2)}{dt}=\frac{\pi a_0^4}{2V_0}\left[\frac{1}{\phi_r}\frac{d\phi}{d\eta}\right]\Bigg|^{\lambda_s}\frac{D}{2\sqrt{Dt}}, \tag{85}$$

so that integrating and using Eq. (45) gives

$$a^2(t)=a_0^2+\frac{\pi\lambda_l a_0^4}{V_0}\left(1-\phi_0-\frac{\lambda_s}{\lambda_l}\right)\sqrt{Dt}. \tag{86}$$

Again note that $\lambda_l<0$ for penetration. This gives the disappearance time (when $a=0$)

$$t_D=\frac{1}{D}\left[\frac{V_0}{\pi\lambda_l a_0^2(1-\phi_0-\lambda_s/\lambda_l)}\right]^2. \tag{87}$$

Finally, we can combine Eq. (86) with the expressions for $h_l(t)$ and $h_s(t)$ in Eq. (34) to find analytical expressions for

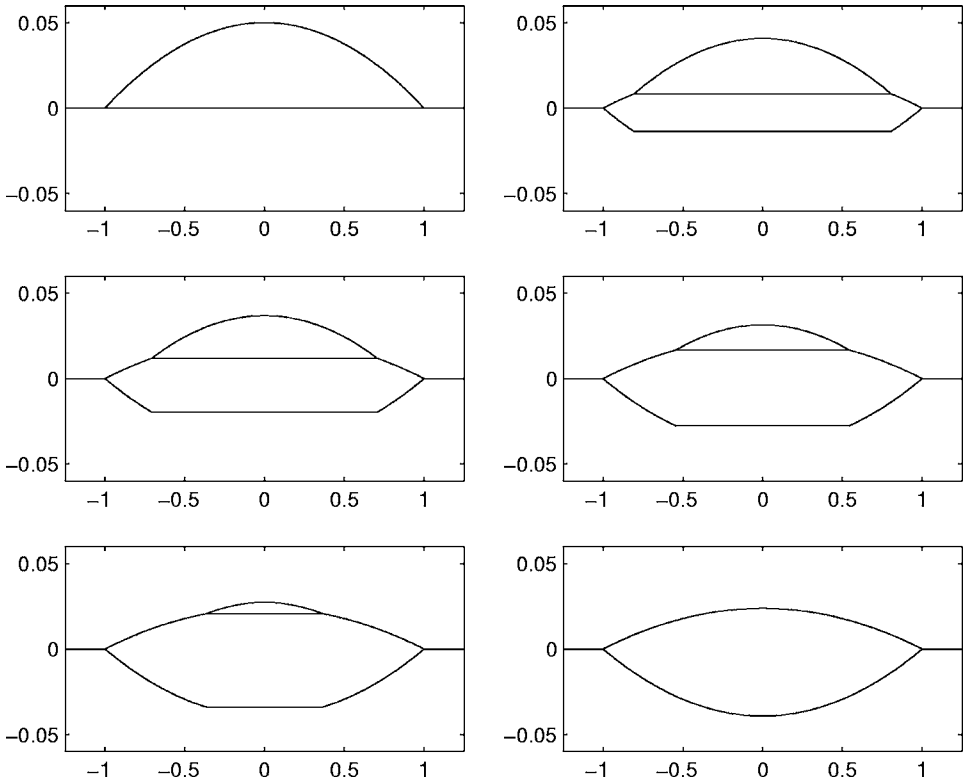

FIG. 7. Model 2A: This figure shows the geometry of the wet substrate region and the liquid droplet for times $t/t_D=0,0.125,0.25,0.5,0.75,1$ (reading left to right first then down) where $t_D=0.0011$. We have used $a_0=1$, $V_0=0.787$, $\phi_0=\phi_l=0.33$, and $\phi_r=0.1$.

the spatial profiles of the liquid penetration and the substrate surface deformation:

$$h_l(r) = -\left[\frac{2V_0}{\pi a_0^4(1-\phi_0-\lambda_s/\lambda_l)}\right](a_0^2-r^2), \tag{88}$$

$$h_s(r) = -\frac{\lambda_s}{\lambda_l}\left[\frac{2V_0}{\pi a_0^4(1-\phi_0-\lambda_s/\lambda_l)}\right](a_0^2-r^2), \tag{89}$$

for $r \geqslant a(t)$. The dependence of these profiles on ϕ_l and ϕ_r enter only through the values of λ_s and λ_l. We again see planar fronts for the substrate deformation and liquid penetration in the interior, and now parabolic profiles in the exterior region as indicated in the example of Fig. 7. As in Model 1A, the solid fraction throughout the wet substrate is nonuniform. As shown in Appendix B, this solution can be generalized to nonslender geometries. The result is that instead of parabolic profiles for the deformation and liquid penetration fronts, one finds elliptical shapes.

The relationship θ_{APP} vs da/dt is qualitatively similar to that shown in Fig. 3 of Davis and Hocking.[7] That is, da/dt tends toward infinity as $t \to 0$ and as $t \to t_D$; that is, θ_{APP} is not a single-valued function of speed in this model.

D. Model 2B: Davis and Hocking droplet model

Here we describe the droplet evolution predictions for the case where the wet substrate region continues to evolve after the overlying liquid has been imbibed and the upper surface of the wet substrate exposed to air. The approach we take in obtaining interface profiles is equivalent to the approach described in Sec. IV B and so a description of the general approach will not be repeated here. We note that a new formula for $t_l(r)$ applies in this case and is given by setting $r=a(t)$ in Eq. (86). In this case we have

$$Dt_l(r) = (r^2-a_0^2)^2\left[\frac{V_0}{\pi\lambda_l a_0^4(1-\phi_0-\lambda_s/\lambda_l)}\right]^2. \tag{90}$$

The analog results of those shown in Fig. 6 for Model 1B are shown in Fig. 8 for Model 2B. The left column of plots has $\phi_l=0.2$, $\phi_0=0.33$, and $\phi_r=0.1$. The center column of plots has $\phi_l=\phi_0=0.33$ and $\phi_r=0.1$. The right column of plots has $\phi_l=0.5$, $\phi_0=0.33$, and $\phi_r=0.1$. A time series is shown in each column with $t/t_D=0.25$, 0.75, 1.5, and 12.0 where $t_D=0.0019$ (column 1), 0.0011 (column 2) and 0.0008 (column 3). The initial configuration for each is a parabolic shape as given in the upper left plot of Fig. 7. Initially swelling occurs in all cases shown since $\lambda_s>0$ but the long term behavior is determined by the relative size of ϕ_l and ϕ_0. Again, when the equilibrium solid fraction is smaller than the original ϕ_0 the wet substrate swells and when the equilibrium solid fraction is larger than the original ϕ_0 the wet substrate shrinks. In the borderline case when $\phi_l=\phi_0$ the final shape of the wet substrate is equivalent to that predicted by Davis and Hocking[7] for imbibition into a rigid substrate.

E. Model 3A: Clarke *et al.* droplet model

Here we investigate a model for imbibition and substrate deformation that implements the relation between the contact line speed and the contact angle used by Clarke *et al.*[2] for spreading on a rigid porous substrate. Specifically, we take

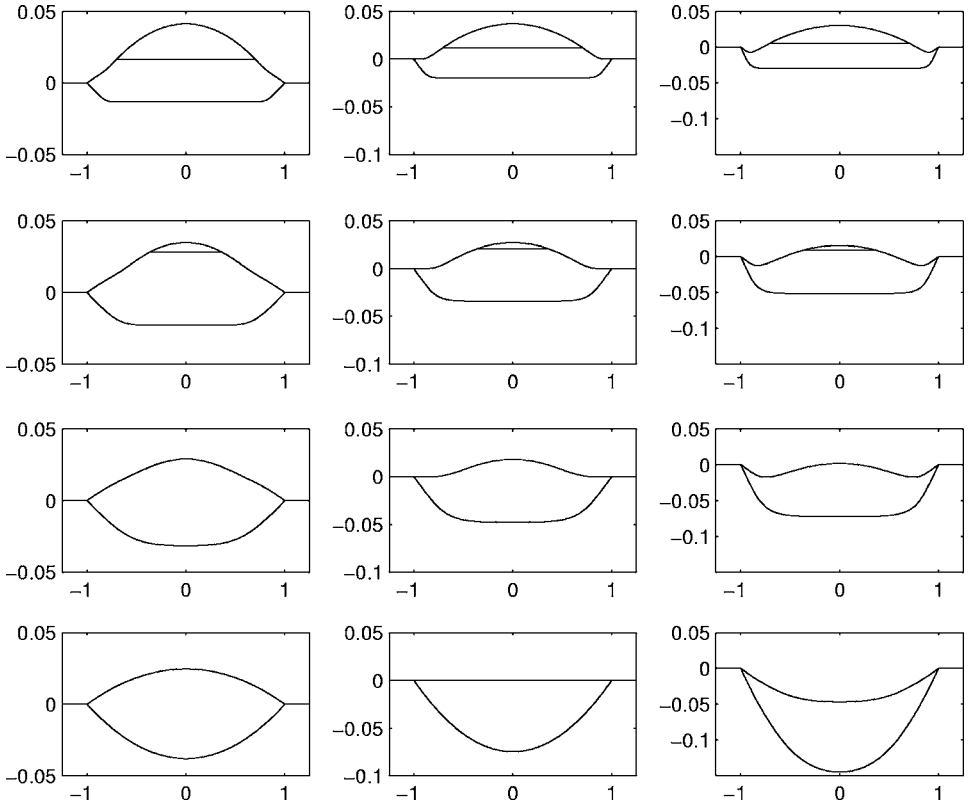

FIG. 8. Model 2B: Three different time series (top to bottom). The left column of plots shows the time series for the case $\phi_l=0.2$, $\phi_0=0.33$, and $\phi_r=0.1$. The center column of plots has $\phi_l=\phi_0=0.33$ and $\phi_r=0.1$. The right column of plots has $\phi_l=0.5$, $\phi_0=0.33$, and $\phi_r=0.1$. The four rows show the four times $t/t_D=0.25$, 0.75, 1.5, and 12.0 where $t_D=0.0019$ (in column 1), 0.0011 (in column 2) and 0.0008 (in column 3). The initial configuration for each is a parabolic shape as given in the upper left plot of Fig. 7. Initially swelling occurs in all cases since $\lambda_s>0$ but the long term behavior is determined by the relative size of ϕ_l and ϕ_0. Additional parameter values are $a_0=1$ and $V_0=0.787$.

$$\frac{da}{dt}=\tilde{\kappa}\sinh[\Gamma(\cos\theta_R-\cos\theta)], \tag{91}$$

where $\tilde{\kappa}=2\kappa_S^0 h\lambda/\mu\nu$ and $\Gamma=\gamma/2nk_BT$. The combination $\xi=\mu nk_BT/\kappa_S^0 h\lambda$ is a "friction" parameter, γ is the liquid surface tension and θ_R is a static receding contact angle. Here we will consider only receding cases, that is, where $da/dt<0$ for all t (see further comments below). We make the spherical cap approximation for the liquid droplet shape so that

$$V_L(t)=\frac{\pi a^3}{3\sin^3\theta}[2-3\cos\theta+\cos^3\theta]. \tag{92}$$

Note that this formula applies as long as the bottom surface of the liquid droplet (i.e., the interface between the wet substrate and the liquid droplet) is planar. The evolution of a, θ and V is closed by the mass conservation condition in Eq. (70), which we can express as

$$\frac{dV_L}{dt}=2\pi a^2\lambda_l(1-\phi_0-\lambda_s/\lambda_l)\frac{D}{2\sqrt{Dt}}. \tag{93}$$

Again we note that these equations describe only the receding case. There are a number of modifications that are required to address the case in which the liquid droplet may spread, or at least spread initially. First, if the droplet spreads initially, there is a delay before which pores at radial positions with $r>R_0$ begin to fill. This can be handled, as shown by Clarke *et al.* by introducing a radial dependent time function $\tau(r)$ defined as the time at which the pore at radius r begins to fill. This would replace the term $\sqrt{Dt}$ in Eq. (93) with $\sqrt{D[t-\tau(r)]}$, for example. Second, when the droplet spreads initially, the wet substrate–liquid interface underneath it is necessarily nonplanar. That is, the interior region with $r<R_0$ begins to swell at $t=0$ while the region with $R_0<r<R(t)$ swells only after some time delay required for the liquid droplet to reach that radial location. This modifies the equation for the remaining liquid volume to a result dependent on the nonplanar shape of the wet substrate–liquid interface. Additionally, with a nonplanar wet substrate–liquid interface, receding occurs along a nonplanar interface and therefore requires a modified definition of the contact angle. We shall not consider these additional spreading scenarios here.

By focusing on the receding case alone, we can highlight the competition between the rate of receding of the droplet and the deformation rate of the substrate (this specific competition is elucidated in more detail below). The previous two models in Secs. IV A and IV C show cases in which two different time dependencies for the contact line position [$a(t)\sim\sqrt{t}$ in Model 1 and $a^2(t)\sim\sqrt{t}$ in Model 2] gave rise to two notably different shape predictions for the deformed substrate. In the present case, the time dependence of $a(t)$ is not known until the above system of equations is solved and so we anticipate a much richer range of shape predictions to be possible. In order to gain a clearer picture of the above system of equations we shall rewrite Eqs. (91)–(93) in a more compact form.

We write Eqs. (91)–(93) in dimensionless form by introducing a length scale a_0, a volume scale a_0^3 and a time scale a_0^2/D. These equations become

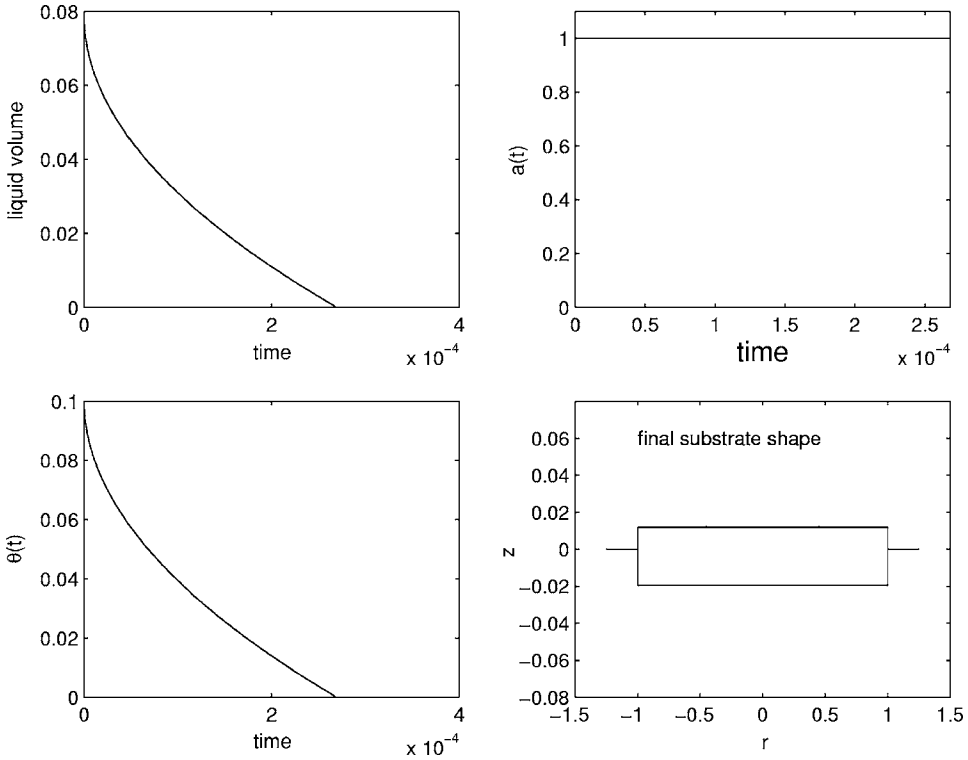

FIG. 9. Model 3A: This figure shows plots of the dynamics of $V_L(t)$, $a(t)$, and $\theta(t)$ and the final deformed substrate shape for the parameter values $K=10$, $\Gamma=0.2$, $\theta_R=0.2$, $\phi_l=\phi_0=0.33$, $\phi_r=0.1$, $\theta_0=0.1$, $V_0=0.0787$. Here $t_D=0.000268$. Note that $V\to 0$ as $\theta\to 0$ with $a\neq 0$.

$$\frac{dV_L}{dt} = -[\lambda_s - (1-\phi_0)\lambda_l]\frac{\pi a^2}{\sqrt{t_0+t}}, \tag{94}$$

$$\frac{da}{dt} = K\sinh[\Gamma(\cos\theta_R - \cos\theta)], \tag{95}$$

$$\frac{d\theta}{dt} = \frac{3}{a^3 g'(\theta)}\left[\frac{dV_L}{dt} - a^2 g(\theta)\frac{da}{dt}\right], \tag{96}$$

where we have differentiated Eq. (92) to obtain the third ODE for $d\theta/dt$. As suggested by Clarke *et al.* we have introduced a small offset time t_0 to avoid numerically the singularity at $t=0$. The new dimensionless parameter appearing here is $K=\tilde{\kappa}a_0/D$, which describes the competition between the rate of receding and the rate of imbibition. In particular, as $K\to 0$ imbibition occurs at a much faster rate than receding while as $K\to\infty$ receding occurs at a much faster rate than imbibition. Estimates for the parameters $\tilde{\kappa}$ and Γ were given by Blake *et al.*[3] They found $\tilde{\kappa}\approx 10^2$ m/s and $\Gamma=0.2$. Additionally, if we use an initial droplet radius of $a_0=10^{-5}$ m and $D\approx 10^{-4}$ m^2/s then $K\approx 10$. In order to highlight different regimes of behavior predicted by this model we shall examine a wide range of values for K. These regimes can be sorted into two general classes. As the liquid volume goes to zero and the droplet is completely imbibed, we find that either $a\to 0$ for nonzero θ or $\theta\to 0$ for nonzero a.

Figure 9 shows the dynamics of $V_L(t)$, $a(t)$, and $\theta(t)$ and the final deformed substrate shape for $K=10$, $\Gamma=0.2$, $\theta_R=0.2$, $\phi_l=\phi_0=0.33$, $\phi_r=0.1$, $\theta_0=0.1$, and $V_0=0.0787$. Due to the rapid imbibition of the liquid droplet the numerical solutions here are insensitive to the changes in K (up to approximately $K=10^4$). In these cases the liquid droplet is immediately imbibed into the substrate with nearly no horizontal motion of the contact line. As the liquid volume goes to zero, the contact angle goes to zero while the contact line position, $a(t)$ remains close to its original value. Consequently, the final wet substrate takes the shape of a circular disk. As K increases further, there is increased motion of the contact line but the final value of $a(t)$ may still be bounded away from zero as $V_L\to 0$ and $\theta\to 0$.

A result for the regime in which $a\to 0$ with nonzero θ as $V_L\to 0$ is shown in Fig. 10 for the same parameter values as for Fig. 9 except that $K=2.4\times 10^6$ and $\theta_R=0.1$ (note $\theta_0=0.1$). Here the contact angle varies nonmonotonically, decreasing initially to a minimum and then increasing monotonically.

The extreme case, when $K\to\infty$ corresponds to the fixed contact angle case. Indeed, Eq. (92) shows that in this case $\theta(t)=\theta_R$ as a leading order approximation. Here after an initial boundary layer as the contact angle transitions from a value of θ_0 to a value of θ_R, the shape predictions are similar to the conical shapes observed in Sec. IV A. The numerical simulations show that this regime is not reached numerically until K is extremely large ($K\approx 10^7$ for $\Gamma=0.2$). In the context of Model 3 then, we interpret Model 1 with constant contact angle as a case in which there is rapid motion of the contact line.

F. Model 3B: Clarke *et al.* droplet model

The model described in the previous section can be adapted in a similar way to that used for Models 1 and 2 in order to allow continued evolution of the wet-substrate region. In this case, rather than identifying an analytical expression for $t_l(r)$ [as in Eqs. (79) and (90)], we obtain a value

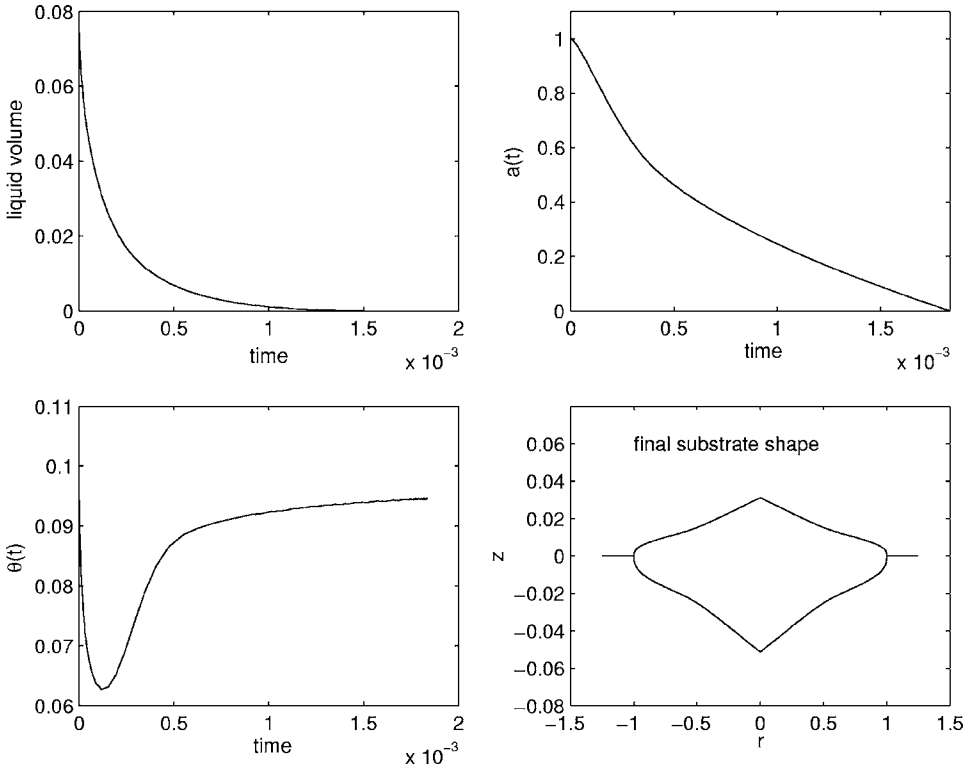

FIG. 10. Model 3A: This figure shows plots of the dynamics of $V_L(t)$, $a(t)$, and $\theta(t)$ and the final deformed substrate shape for the parameter values $K=2.4\times10^6$, $\Gamma=0.2$, $\theta_R=0.1$, $\phi_l=\phi_0=0.33$, $\phi_r=0.1$, $\theta_0=0.1$, $V_0=0.0787$. Here $t_D=0.0019$. Note that $V\to0$ as $a\to0$ with $\theta\neq0$.

for the imbibition time at a given radial position from the numerical solution vectors for t and a as $r=a(t_I)$. We again use cubic splines to evaluate the required t_I values from the discrete set obtained by the numerical integration.

Figure 11 shows the evolution of the liquid and substrate for three sets of parameter values. The left column of plots has $\phi_l=0.2$, $\phi_0=0.33$, and $\phi_r=0.1$. The center column of plots has $\phi_l=\phi_0=0.33$ and $\phi_r=0.1$. The right column of plots has $\phi_l=0.5$, $\phi_0=0.33$, and $\phi_r=0.1$. The main conclusions here are again that the wet substrate is eventually expanded if $\phi_l<\phi_0$, contracted if $\phi_l>\phi_0$ and undeformed if $\phi_l=\phi_0$. Owing to the relatively large value of K used in these calculations which has the effect of allowing only small changes in the value of the contact angle, the shapes here are more characteristic of the constant contact angle results observed in Model 1B (see Fig. 6).

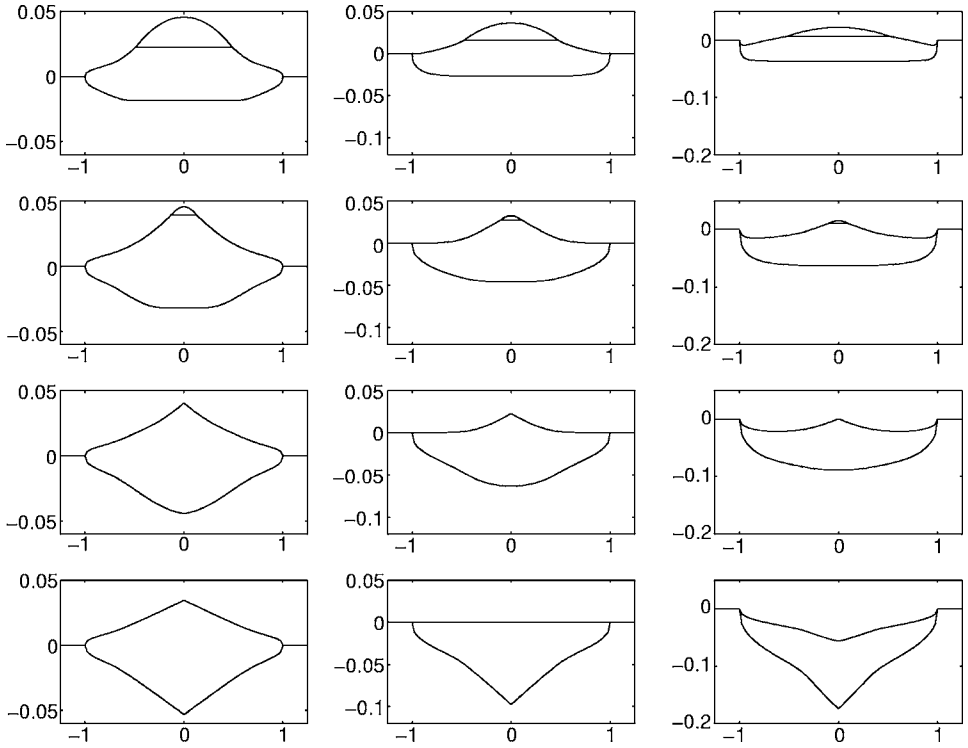

FIG. 11. Model 3B: Three different time series (top to bottom). The left column of plots shows the time series for the case $\phi_l=0.2$, $\phi_0=0.33$, and $\phi_r=0.1$. The center column of plots has $\phi_l=\phi_0=0.33$ and $\phi_r=0.1$. The right column of plots has $\phi_l=0.5$, $\phi_0=0.33$, and $\phi_r=0.1$. The four rows show the four times $t/t_D=0.25$, 0.75, 1.5, and 12.0 where $t_D=0.0037$ (in column 1), 0.0019 (in column 2) and 0.0012 (in column 3). The initial configuration for each is a spherical cap shape as given in the upper left plot of Fig. 5. Initially swelling occurs in all cases since $\lambda_s>0$ but the long term behavior is determined by the relative size of ϕ_l and ϕ_0. Additional parameter values are $K=2.4\times10^6$, $\Gamma=0.2$, $\theta_R=0.1$, $\theta_0=0.1$, $V_0=0.0787$.

V. CONCLUSIONS

We have shown that relatively simple models for the interaction between a liquid droplet and a deformable porous substrate can be derived and solved. These models couple a one-dimensional description of imbibition into a deformable porous medium to models for the liquid droplet dynamics.

The one-dimensional deformation model used here is based on the model of Preziosi *et al.*[22] and is similar to several other related models.[12,21,33,47] In the present work we have identified a nearly analytical solution to the one-dimensional deformation problem with simple but representative constitutive equations for the permeability and stress functions appearing in the deformation model. These functions are input to the deformation model and in principle could be modified and improved for specific systems. We have specifically identified a one-dimensional deformation model for a finite fluid volume. While the infinite volume case predicts deformation and penetration fronts that grow indefinitely, our model for a finite fluid volume predicts deformation initially and then relaxation back to a state with uniform solid fraction. During the imbibition process a similarity solution governs the dynamics of the flow. For small solid fraction values ϕ_l the upper surface of the substrate rises and the substrate swells while the fluid penetrates into the substrate. For very large solid fraction values ϕ_l the upper surface of the substrate becomes depressed and the substrate shrinks. Interestingly, the transition from swelling to shrinking based on this criterion differs from that based on a long-time equilibrium solution in which the solid fraction (as well as pressure and stress) in the wet substrate is uniform. This leads to the identification of four notable regimes: (i) the substrate swells initially and eventually relaxes to an expanded configuration leaving a bump on the substrate surface, (ii) the substrate swells initially and eventually relaxes to an undeformed configuration leaving a perfectly flat substrate surface, (iii) the substrate expands initially but ultimately relaxes to a compacted configuration leaving a pit along the substrate surface, and (iv) the substrate shrinks initially and ultimately relaxes to a compacted state with a pit along the substrate surface.

We have investigated the coupling of the droplet imbibition and one-dimensional substrate deformation to three different models for the droplet evolution. For each of these three models we have shown solutions for two different scenarios involving evolution of the wet substrate–air interface; Case A freezes all further evolution and Case B allows further evolution based on the assumption that the wet substrate–air interface neither dries out nor disappears under a puddle. In Case A, the final state involves a deformed substrate characteristic of the similarity solution described for the one-dimensional imbibition and substrate penetration. Here the solid fraction is "frozen in" at the appearance of the wet substrate–air interface and is nonuniform throughout the wet substrate. In Case B, deformation of the substrate occurs during the imbibition process and a relaxation of this deformation back to a state of uniform pressure, stress and solid fraction continues after the droplet has been completely imbibed. While the initial growth is governed by the dynamics of the similarity solution, generally the final equilibrium state (expanded, contracted or undeformed) depends on the value of ϕ_l; if $\phi_l < \phi_0$ the end result is swollen substrate, if $\phi_l = \phi_0$ then end result is an undeformed substrate and if $\phi_l > \phi_0$ then the end result is a shrunken substrate.

The primary effect of the specific droplet dynamics model lies not in whether or not the substrate swells, shrinks or remains undeformed but in the details of the predicted shape. In Model 1 (constant contact angle) the substrate shapes (deformed or undeformed) have conical features. In Model 2 (Hocking and Davis model with constant curvature) the substrate shapes are characterized by parabolic features. In Model 3 (Clarke *et al.* model) two characteristic regimes are observed. The regime of "fast" receding is characteristic of the constant contact angle case where $a \to 0$ as $V_L \to 0$ (and $\theta \neq 0$) while the regime of "slow" receding can be related to a fixed contact line case where $\theta \to 0$ as $V_L \to 0$ (and $a \neq 0$). Generally, we find receding retards imbibition. This can be understood by noting that the quantity of fluid taken up by the substrate is proportional to the contact area (and hence the radial position of the contact line squared). These two limiting cases noted above for a deformable substrate are the same as the "decreased drawing area" (fixed contact angle) and the "constant drawing area" (fixed contact line) examined by Denesuk *et al.*[45,46] for a rigid substrate. The trend for disappearance time observed by those authors is the same as that observed for the present case. Models 2A and 2B described in Secs. IV C and IV D on the one hand represents a borderline case (where $a \to 0$ and $\theta \to 0$ as $V_L \to 0$). However, as pointed out by Davis and Hocking[7] the corresponding relationship between da/dt and θ at the contact line in their model is nonmonotonic and therefore we conclude must necessarily be distinct from Model 3.

Clearly there is an opportunity for experimental work on these systems. We have derived solutions in the most simple case—one-dimensional imbibition and deformation of an initially static liquid droplet. Additional complications such as multispecies effects, evaporation and other drying processes, fully two-dimensional deformation effects, and chemical interaction between the liquid and solid phases may be required to connect with observations in actual systems. Our hope is that experimental investigations and more sophisticated models may be motivated by the present work.

ACKNOWLEDGMENTS

D.M.A. acknowledges support from the 3M Non-Tenured Faculty Award Program, the Faculty Summer Research Support Program at George Mason University, and NSF Award No. DMS-0306996. The author would also like to thank D. A. Huntley and S. Mohanty at 3M Corporation for initially suggesting the investigation of this problem and A. A. Wheeler for helpful discussions in the early stages of this work.

APPENDIX A: FINITE VOLUME IMBIBITION TIME

Here we calculate an expression for the time for complete imbibition of a finite volume of fluid penetrating into a

deformable substrate. This calculation extends the results in Sec. III D.

In particular, if we denote $\bar{V}(t)$ as the volume per unit area of the supply of fluid above the substrate, then its rate of change can be related to the volume flux into the substrate:

$$\frac{d\bar{V}}{dt} = (1-\phi)(w_l - w_s)\big|_{z=h_s}. \tag{A1}$$

Using the one-dimensional flow results we find that

$$\frac{d\bar{V}}{dt} = \frac{D}{\phi}\left.\frac{\partial\phi}{\partial z}\right|_{h_s} = \frac{D}{\phi}\frac{1}{2\sqrt{Dt}}\left.\frac{d\phi}{d\eta}\right|_{\eta=\lambda_s}. \tag{A2}$$

This equation has the solution

$$\bar{V}(t) = V_0 + \frac{1}{\phi}\left.\frac{d\phi}{d\eta}\right|_{\eta=\lambda_s}\sqrt{Dt}, \tag{A3}$$

where V_0 is the initial ($t=0$) volume per unit area (height) of the overlying fluid. We can simplify this using expression (45) to find that

$$\bar{V}(t) = V_0 + 2[(1-\phi_0)\lambda_l - \lambda_s]\sqrt{Dt}. \tag{A4}$$

Using this result we can define the time, t_I at which the supply of liquid has been completely imbibed into the substrate [when $\bar{V}(t_I)=0$]. We find that

$$Dt_I = \left(\frac{V_0}{2[(1-\phi_0)\lambda_l - \lambda_s]}\right)^2. \tag{A5}$$

APPENDIX B: MODEL 2A—NONSLENDER GEOMETRIES

Note that one can generalize the solution presented in Sec. IV C to nonslender geometries if one still imposes the spherical cap approximation on the liquid droplet shape. In this case the final deformation and penetration fronts are elliptical rather than parabolic. This result holds for liquid droplets with contact angles of less than 90 degrees (so that as the droplet is imbibed the contact line position decreases monotonically to zero). We describe this solution below.

Suppose that the liquid droplet position is parametrized by $r=R_L(z,t)$. Then a spherical cap approximation can be written as

$$R_L^2 + \left[z - a\tan\left(\theta - \frac{\pi}{2}\right)\right]^2 = \frac{a^2}{\sin^2\theta} \tag{B1}$$

(for example, see Anderson, Forest, and Superfine[50]). A solution that maintains constant curvature in space and time has

$$\frac{a}{\sin\theta} = \frac{a_0}{\sin\theta_0}, \tag{B2}$$

where a_0 and θ_0 are the initial contact line position and initial contact angle. We assume that $\theta_0 < \pi/2$. The liquid volume in this case is given by Eq. (92). One can derive by differentiating Eq. (92) and using Eq. (B2) that

$$\frac{dV}{dt} = \pi a^3\frac{d\theta}{dt}. \tag{B3}$$

Now using this result and Eq. (93) we find that

$$\pi a^2[(1-\phi_0)\lambda_l - \lambda_s]\frac{D}{\sqrt{Dt}} = \pi a^3\frac{d\theta}{dt}. \tag{B4}$$

Upon using Eq. (B2) one obtains

$$-\frac{\sin\theta_0}{a_0}[(1-\phi_0)\lambda_l - \lambda_s]\frac{D}{\sqrt{Dt}} = \frac{d}{dt}\cos\theta. \tag{B5}$$

This equation can be solved to obtain

$$\cos\theta = \cos\theta_0 - \frac{\sin\theta_0}{a_0}[(1-\phi_0)\lambda_l - \lambda_s]2\sqrt{Dt}. \tag{B6}$$

Now using $a^2 = a_0^2(1-\cos^2\theta)/\sin^2\theta_0$, $h_l = 2\lambda_l\sqrt{Dt}$ and $h_s = 2\lambda_s\sqrt{Dt}$ we write down expressions for the penetration and substrate deformation profiles (equating a with radial position r)

$$r^2 + \left[\frac{a_0\cos\theta_0}{\sin\theta_0} - \frac{[(1-\phi_0)\lambda_l - \lambda_s]}{\lambda_s}h_s(r)\right]^2 = \frac{a_0^2}{\sin^2\theta_0}, \tag{B7}$$

$$r^2 + \left[\frac{a_0\cos\theta_0}{\sin\theta_0} - \frac{[(1-\phi_0)\lambda_l - \lambda_s]}{\lambda_l}h_l(r)\right]^2 = \frac{a_0^2}{\sin^2\theta_0}. \tag{B8}$$

These are elliptical profiles.

APPENDIX C: CASE A—AVERAGE SOLID FRACTION

We note that in the droplet penetration/deformation model in Case A the solid fraction and interface positions are frozen for $r \geq a(t)$. This fixes a solid fraction distribution in the wet substrate which is not uniform and in the model of Case B continues to drive a flow and cause motion of the boundaries. Here we investigate some properties of the "frozen in" solid fraction distribution of Case A. We can determine $\phi(r,z)$ using the solution $\phi(\eta)$ with suitable interpretation of $\eta = z/2\sqrt{Dt}$. If we interpret $\eta = \eta(z,t)$ with $t = a^{-1}(r)$ [a^{-1} being the inverse function of $a(t)$], where

$$t = a^{-1}(r) = \frac{(r-a_0)^2}{D}\left[\frac{g(\theta)}{2\pi\lambda_l(1-\phi_0-\lambda_s/\lambda_l)}\right]^2, \quad \text{for Model 1A,} \tag{C1}$$

$$t = a^{-1}(r) = \frac{(r^2-a_0^2)^2}{D}\left[\frac{V_0}{\pi\lambda_l a_0^4(1-\phi_0-\lambda_s/\lambda_l)}\right]^2, \quad \text{for Model 2A,} \tag{C2}$$

then the final distribution of ϕ in the wet substrate is given by $\phi(r,z) = \phi\{\eta[z, a^{-1}(r)]\}$ where $h_l(r) \leq z \leq h_s(r)$ and $0 \leq r \leq a_0$. We have confirmed by direct integration of Eq. (12) that $V^*(t_D) = V_0$. In this calculation we note that

$$
\begin{aligned}
&2\pi\int_0^{a_0}\int_{h_l(r)}^{h_s(r)} r\phi(r,z)dz\,dr \\
&\quad = 2\pi\left[\int_{\lambda_l}^{\lambda_s}\phi(\eta)d\eta\right]\left[\int_0^{a_0} 2\sqrt{Dt}\,dr\right] \\
&\quad = 2\pi[-\lambda_l\phi_0]\left[-\frac{V_0}{2\pi\lambda_l(1-\phi_0-\lambda_s/\lambda_l)}\right] \\
&\quad = \frac{\phi_0 V_0}{(1-\phi_0-\lambda_s/\lambda_l)},
\end{aligned}
\tag{C3}
$$

where $t=a^{-1}(r)$ is given by Eqs. (C1) and (C2).

As we have seen in Secs. IV A and IV C analytical predictions of the interface positions given by Eqs. (77) and (88) have been obtained. Given these final shapes of the wet and deformed substrate we can calculate the volume occupied by the wet substrate region $V_S(t_D)$ (this includes both solid and liquid). For both of these models we find that

$$
V_S(t_D) = \frac{1-\lambda_s/\lambda_l}{1-\phi_0-\lambda_s/\lambda_l}V_0, \tag{C4}
$$

where V_0 is the initial liquid volume. This formula allows us to identify an average solid fraction in the wet substrate by noting that the factor multiplying V_0 can be interpreted as $1/(1-\phi_{ave})$ where

$$
\phi_{ave} = \frac{\phi_0}{1-\lambda_s/\lambda_l}. \tag{C5}
$$

This can also be confirmed by directly averaging $\phi(r,z)$ over the final volume V_S [using Eqs. (C3) and (C4)]. Using the $\lambda_s=0.3646$, $\lambda_l=-0.5993$, $\phi_r=0.1$, and $\phi_l=\phi_0=0.33$ we find that $\phi_{ave}\approx 0.21$ which falls between the values $\phi_r=0.1$ and $\phi_l=0.33$.

[1] E. W. Washburn, "The dynamics of capillary flow," Phys. Rev. **17**, 273 (1921).
[2] A. Clarke, T. D. Blake, K. Carruthers, and A. Woodward, "Spreading and imbibition of liquid droplets on porous surfaces," Langmuir **18**, 2980 (2002).
[3] T. D. Blake, A. Clarke, J. De Coninck, and M. J. de Ruijter, "Contact angle relaxation during droplet spreading: Comparison between molecular kinetic theory and molecular dynamics," Langmuir **13**, 2164 (1997).
[4] R. K. Holman, M. J. Cima, S. A. Uhland, and E. Sachs, "Spreading and infiltration of inkjet-printed polymer solution droplets on a porous substrate," J. Colloid Interface Sci. **249**, 432 (2002).
[5] M. Sami Selim, V. F. Tesavage, R. Chebbi, and S. H. Sung, "Drying of water-based inks on plain paper," J. Imaging Sci. Technol. **41**, 152 (1997).
[6] S. H. Davis and L. M. Hocking, "Spreading and imbibition of viscous liquid on a porous base," Phys. Fluids **11**, 48 (1999).
[7] S. H. Davis and L. M. Hocking, "Spreading and imbibition of viscous liquid on a porous base. II," Phys. Fluids **12**, 1646 (2000).
[8] V. M. Starov, S. R. Kosvintsev, V. D. Sobolev, M. G. Verlarde, and S. A. Zhdanov, "Spreading liquid drops over saturated porous layers," J. Colloid Interface Sci. **246**, 372 (2002).
[9] D. Seveno, V. Ledauphin, G. Martic, M. Voué, and J. De Conninck, "Spreading drop dynamics on porous surfaces," Langmuir **18**, 7496 (2002).
[10] J. F. Oliver, L. Agbezuge, and K. Woodcock, "A diffusion approach for modelling penetration of aqueous liquids into paper," Colloids Surf., A **89**, 213 (1994).
[11] J. Ghassemzadeh, M. Hashemi, L. Sartor, and M. Sahimi, "Pore network simulation of imbibition into paper during coating: I. Model development," AIChE J. **47**, 519 (2001).
[12] M. Spiegelman, "Flow in deformable porous media. Part 1. Simple analysis," J. Fluid Mech. **247**, 17 (1993).
[13] T. K. Karalis, "Water flow in non-saturated swelling soil," Int. J. Eng. Sci. **31**, 751 (1993).
[14] S. Achanta, J. H. Cushman, and M. R. Okos, "On multicomponent, multiphase thermomechanics with interfaces," Int. J. Eng. Sci. **32**, 1717 (1994).
[15] M. A. Murad, L. S. Bennethum, and J. H. Cushman, "A multi-scale theory of swelling porous media: I. Application to one-dimensional consolidation," Transp. Porous Media **19**, 93 (1995).
[16] L. S. Bennethum and T. Giorgi, "Generalized Forchheimer equation for two-phase flow based on hybrid mixture theory," Transp. Porous Media **26**, 261 (1997).
[17] M. Kaczmarek and T. Hueckel, "Chemico-mechanical consolidation of clays: Analytical solutions for a linearized one-dimensional problem," Transp. Porous Media **32**, 49 (1998).
[18] D. W. Smith, "One-dimensional contaminant transport through a deforming porous medium: Theory and a solution for a quasi-steady-state problem," Int. J. Numer. Analyt. Meth. Geomech. **24**, 693 (2000).
[19] M. Kaczmarek, "Chemically induced deformation of a porous layer coupled with advective-dispersive transport. Analytical solutions," Int. J. Numer. Analyt. Meth. Geomech. **25**, 757 (2001).
[20] G. P. Peters and D. W. Smith, "Solute transport through a deforming porous medium," Int. J. Numer. Analyt. Meth. Geomech. **26**, 683 (2002).
[21] J. L. Sommer and A. Mortensen, "Forced unidirectional infiltration of deformable porous media," J. Fluid Mech. **311**, 193 (1996).
[22] L. Preziosi, D. D. Joseph, and G. S. Beavers, "Infiltration of initially dry, deformable porous media," Int. J. Multiphase Flow **22**, 1205 (1996).
[23] V. J. Michaud, J. L. Sommer, and A. Mortensen, "Infiltration of fibrous performs by a pure metal: Part V. Influence of preform compressibility," Metall. Mater. Trans. A **30**, 471 (1999).
[24] D. Ambrosi and L. Preziosi, "Modeling injection molding processes with deformable porous preforms," SIAM J. Appl. Math. **61**, 22 (2000).
[25] L. Billi and A. Farina, "Unidirectional infiltration in deformable porous media: Mathematical modeling and self-similar solution," Q. Appl. Math. **58**, 85 (2000).
[26] K. S. A. Chen and L. E. Scriven, "Liquid penetration into a deformable porous substrate," Tappi J. **73**, 151 (1990).
[27] A. D. Fitt, P. D. Howell, J. R. King, C. P. Please, and D. W. Schwendeman, "Multiphase flow in a roll press nip," Eur. J. Appl. Math. **13**, 225 (2002).
[28] M. H. Holmes, "A nonlinear diffusion equation arising in the study of soft tissue," Q. Appl. Math. **41**, 209 (1983).
[29] M. H. Holmes, "Comparison theorems and similarity solution approximations for a nonlinear diffusion equation arising in the study of soft tissue," SIAM J. Appl. Math. **44**, 545 (1984).
[30] M. H. Holmes, "A theoretical analysis for determining the nonlinear hydraulic permeability of a soft tissue from a permeation experiment," Bull. Math. Biol. **47**, 669 (1985).
[31] M. H. Holmes, "Finite deformation of soft tissue: analysis of a mixture model in uni-axial compression," J. Biomech. Eng. **108**, 372 (1986).
[32] M. H. Holmes and V. C. Mow, "The nonlinear characteristics fo soft gels and hydrated connective tissue in ultrafiltration," J. Biomech. **23**, 1145 (1990).
[33] S. I. Barry and G. K. Aldis, "Flow-induced deformation from pressurized cavities in absorbing porous tissues," Bull. Math. Biol. **54**, 977 (1992).
[34] T. G. Myers, G. K. Aldis, and S. Naili, "Ion induced deformation of soft tissue," Bull. Math. Biol. **57**, 77 (1995).
[35] C. Zoppou, S. I. Barry, and G. N. Mercer, "Dynamics of human milk extraction: A comparative study of breast feeding and breast pumping," Bull. Math. Biol. **59**, 953 (1997).
[36] X-Y. Zhang, J. Luck, M. W. Dewhirst, and F. Yuan, "Interstitial hydraulic conductivity in a fibrosarcoma," Am. J. Physiol. Heart Circ. Physiol. **279**, H2726 (2000).
[37] S. McGuire and F. Yuan, "Quantitative analysis of intratumoral infusion of color molecules," Am. J. Physiol. Heart Circ. Physiol. **281**, H715 (2001).
[38] N. L. Thomas and A. H. Windle, "A theory of case II diffusion," Polymer **23**, 529 (1982).
[39] M. A. Biot, "General theory of three-dimensional consolidation," J. Appl. Phys. **12**, 155 (1941).
[40] M. A. Biot, "Consolidation settlement under a rectangular load distribution," J. Appl. Phys. **12**, 426 (1941).
[41] M. A. Biot and F. M. Clingan, "Consolidation settlement of a soil with an

imperveous top surface," J. Appl. Phys. **12**, 578 (1941).
[42] A. Marmur, "The radial capillarity," J. Colloid Interface Sci. **124**, 301 (1988).
[43] A. Borhan and K. K. Rungta, "An experimental study of the radial penetration of liquids in thin porous substrates," J. Colloid Interface Sci. **158**, 403 (1993).
[44] A. Marmur, "Drop penetration into a thin porous medium," J. Colloid Interface Sci. **123**, 161 (1988).
[45] M. Denesuk, G. L. Smith, B. J. J. Zelinski, N. J. Kreidl, and D. R. Uhlmann, "Capillary penetration of liquid droplets into porous materials," J. Colloid Interface Sci. **158**, 114 (1993).
[46] M. Denesuk, B. J. J. Zelinski, N. J. Kreidl, and D. R. Uhlmann, "Dynamics of incomplete wetting on porous materials," J. Colloid Interface Sci. **168**, 142 (1994).
[47] S. I. Barry and G. K. Aldis, "Radial flow through deformable porous shells," J. Aust. Math. Soc. Ser. B, Appl. Math. **34**, 333 (1993).
[48] D. M. Anderson, R. M. McLaughlin, and C. T. Miller, "The averaging of gravity currents in porous media," Phys. Fluids **15**, 2810 (2003).
[49] D. M. Anderson, M. G. Worster, and S. H. Davis, "The case for a dynamic contact angle in containerless solidification," J. Cryst. Growth **163**, 329 (1996).
[50] D. M. Anderson, M. G. Forest, and R. Superfine, "A model for a spreading and melting droplet on a heated substrate," SIAM J. Appl. Math. **61**, 1502 (2001).